PDEng Report

DEVELOPMENT OF A HAPTIC MOBILE INDUSTRIAL LIFTING AID

MICHEL A. VAN HIRTUM

September, 2017

FACULTY OF ENGINEERING TECHNOLOGY
LABORATORY OF BIOMECHANICAL ENGINEERING

Graduation commission:
Prof. Dr. Ir. H. van der Kooij
Prof. Dr. Ir. H.F.J.M. Koopman
Dr. Ir. T.H.J Vaneker
Ing. F. Tönis

Development of a haptic mobile industrial lifting aid,
September 2017

PREFACE

The development of the WingMAS and AGB would not be possible without the help and support of numerous individuals. Therefore I would like to start thanking some of them.

First, I would like to express my gratitude to Arno Stienen who created the possibility for this PDEng assignment. His guidance and enthusiasm during the whole project was really helpful.

Furthermore, I would like to thank my daily supervisor Arvid Keemink. He was of great help, especially with the most complex challenges.

A special thanks Hankamp Gears, the company who collaborated with the University of Twente for making this PDEng project possible. Thanks to Freek Tonis for his determination and confidence in the project. In addition, thanks to Koen Heuver for his help on many prototypes, in particular his work on the early mechanical design for AGB.

Lastly, I would like to thank the students Nienke Bink, Joeri Landman, Ralph Macke, Ewoud Velu and Louise Schneider for their work and commitment on this project.

ABSTRACT

One out of five Dutch employees indicated that they had to perform frequent heavy lifting and 840.000 employees indicated regular lifting over 25 kg at work. Research showed that frequent heavy lifting increases risks of physical injuries. Lifting aids as cranes and fork lifts are rarely used for payloads weighing less than 25 kg because they are not at immediate disposal. Therefore there is a necessity for a mobile human augmentation device for pick and place operations at the work floor.

A full body exoskeleton was developed with the purpose of completely removing physical strain from the operator while performing pick and place operations. The exoskeleton provides (semi-)passive support which is always at disposal. It contains leg, trunk and arm support. The novel leg parallelogram is responsible for both leg as trunk support. The structure transfers the forces and moment of the payload to the ground. Various options for hand interfaces were evaluated, e.g. gloves with integrated FSRs or a gripper with electromagnets. Moreover, a concept is presented where the backplate is removed for increased moveability.

The arm support contains an automatically adjustable gravity balancer which is able to adjust the compensation from 0 to 20 kg within one second. The gravity balancer is able to provide passive compensation independent of the end point position. A compact design could be realised by using two springs in series. Furthermore, a novel safety mechanism was devised which provides absolute safety, even during a power cut or motor malfunctioning. The dynamic end stop entails a pin which movement is constrained by a slot. The slot follows the pin at a constrained velocity and is self-locking.

The exoskeleton prototype demonstrated the working principles of a (semi-)passive full body exoskeleton. Nevertheless, it was deemed impractical due to constrained range of motion, high weight and long donning and doffing times. The developed arm support on a cart has great premise and for both industrial as clinical usage.

SAMENVATTING

Een op de vijf Nederlandse werknemers heeft aangeven geregeld zwaar te moeten tillen op het werk en 840.000 werknemers gaven aan dat ze zelfs regelmatig meer dan 25 kg tillen. Onderzoek heeft uitgewezen dat regelmatig tillen een serieus gezondheidsrisico met zich meebrengt. Tilhulpen zoals kranen en heftrukken worden zelden gebruikt voor gewichten onder de 25 kg omdat ze niet onmiddellijk beschikbaar zijn. Er bestaat daarom de behoefte aan een mobiele tilhulp die de werknemer ondersteund tijdens pick and place handelingen op de werkvloer.

Een exoskelet was ontwikkeld met de bedoeling om de druk op het lichaam weg te nemen bij het uitvoeren van een pick en place handeling. Het exoskelet biedt (semi-)passieve ondersteuning en is altijd beschikbaar. Het bevat been, romp en arm ondersteuning. Het paralellogram rondom het een is zowel verantwoordelijk voor de been als romp ondersteuning. De structuur leidt de krachten en het moment af naar de grond. Verscheidende mogelijkheden voor hand interfaces zijn geëvalueerd, bijvoorbeeld een handschoen met geïntrigeerde FSRs en een elektromagnetische gripper.

De armondersteuning bevat een automatisch aanpasbare zwaartekracht balanceerder, die compensatie aanpassingen van 0 tot 20 kg binnen een seconde mogelijk maakt. De zwaartekracht balanceerder kan passieve ondersteuning bieden onafhankelijk van de eindpunt positie. Een compact ontwerp kon gerealiseerd worden door twee veren in serie te plaatsen. Een nieuw veiligheidsmechanisme is ontwikkeld wat zelfs veiligheid biedt bij stroom- of aansturingsstoringen. De dynamische eindstop bevat een pin wiens beweging wordt beperkt door een sleuf. De sleuf volgt de pin met een beperkte ingestelde snelheid.

Het exoskelet prototype heeft de werking van een (semi-)passieve volledig exoskelet aangetoond. Desondanks werd het onpraktisch geacht, onder andere de beperkte bewegingsvrijheid, het gewicht en de aan- en uittrek tijd. De ontwikkelde armondersteuning geïnstalleerd op een mobiel frame heeft potentie voor zowel industriel als clinisch gebruik.

CONTENTS

1

GENERAL INTRODUCTION

The PDEng project is part of the sub-programme 'Shared control for a lifting aid' within the STW funded programme H-Haptics. Three companies are involved: Hankamp Gears, Laevo and Siza. The programme explores possibilities for a mechatronic lifting aid for both industry as medical applications. Patient lifting is a physical demanding tasks for nurses and therefore is a need for a lifting aid in health care. Similarly, lifting on the factory floor frequently results in injuries. Therefore, there is a great need for a lifting aid which could reduce work related injuries.

The research group in Enschede is focussed on a lifting aid which suitable for industry and in particular for employees at Hankamp Gears. The consortium in Delft is focussed on patient carrying.

1.1 WORK RELATED INJURIES

(a) (b)

Figure 1: (a) Reishauwer gear grinder. (b) Gear fitting of Reishauwer gear grinder.

One out of five Dutch employees indicated that they had to perform frequent heavy lifting and 840.000 employees indicated regualar lifting over 25 kg [12]. Research showed that frequent lifting has a serious risks of physical injuries [12, 6]. There are no specific guidelines in the Netherlands for lifting at work. The work code refers to the (revised) NIOSH lifting equation [37]. This is a calculation based on scientific research on work related injuries [23, 12].

At Hankamp Gears the placement and removal of the gears into the machines is a physical demanding task. The fitting is usually deep into the machine and with gear weights up to 30 kg this logically results in shoulder and back complains. Although the

lifted weights remain within government regulation, repetitive and unergonomic postures result in physical stress. The burden is highest with older employees and they would therefore benefit most from a lifting aid, as it would enable them to maintain longer in their function. Employee injuries also negatively effects the employers with for example lower efficiency, absenteeism or even occupational disability. In addition, machines will run more efficiently as a result of shorter load and unloading durations.

1.2 PREVIOUS WORK

The goal of the H-Haptics sub-programme is to develop a haptic industrial lifting device.

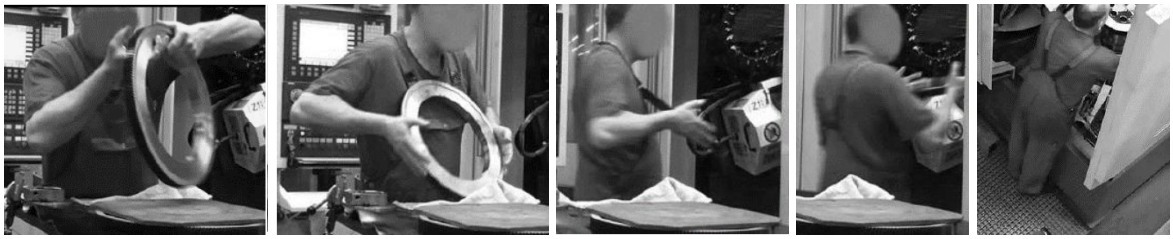

(a) (b) (c) (d) (e)

Figure 2: Motion analysis of loading gears into the grinding machine [24]. (a) Initiating lifting. (b) Transferring hands to bilateral holding. (c) Rotating gear while using chest as pivot point. (d) Reaching for fitting. (e) Placing product on fitting.

The most important scenario for this project is *'loading the grinding machine by the operator'*. Many different machines are stationed at Hankamp Gears, most machines could be categorized as a grinding, milling or lathing machine. Only few can operate fully automatically (loaded and unloaded by a robotic arm), most machines require manual loading and unloading. The gear fitting are unfortunately far into the machines which makes loading an unergonomic tasks. This is most severe with the grinding machine Reishauer RZ400, shown in Figure 1. The movements for loading the grinding machine were analaysed by Pijper [24]. The steps for loading the gear grinder are given in Figure 2.

Initially, it was aimed to develop a static haptic lifting aid to support the gear grinder employee at Hankamp Gears. The concept entailed a gravity balancer; a mechanism with a spring configured in a manner that the end point is statically balanced in 3 DOF space. Three students developed mechanical designs (see Figure 3) for a gravity balancer positioned near the gear grinder:

- *2D lifting aid concept*
  Ideal spring balancer concept by Heuver has a maximum payload of 50 kg and a working area of 1.5 m vertically and 1 m horizontally [15].

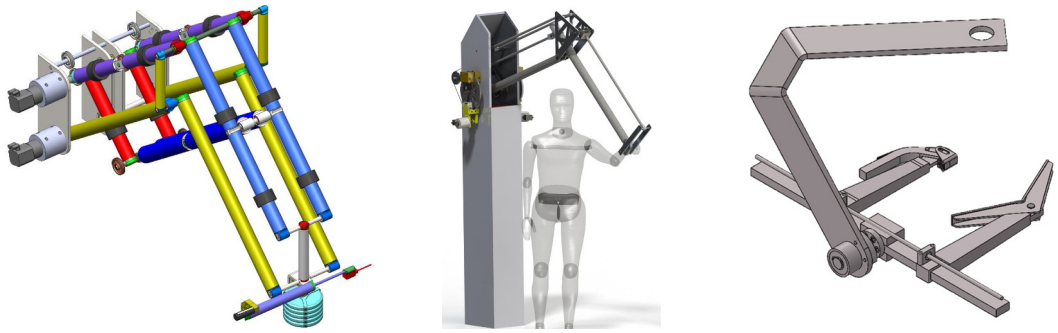

(a) (b) (c)

Figure 3: Concept lifting aids designed by students. (a) 2D lifting aid concept [15]. (b) 3D lifting aid concept [26]. (c) Gear gripper concept [29].

- *3D lifting aid concept*
  Ideal spring balancer concept by Rosendaal [26]. Working principles are similar to the previous concept. Its payload is 20 kg and the working area is 1 m horizontally and 2 m vertically. It features an additional DOF, rotation in the horizontal plane and safety is provided with added disk brakes.

- *Gear gripper concept*
  This gripper is designed by Schuurman to pick and place gears both in horizontal and vertical machine fittings [29]. The design contains a gimbal mechanism and a frictional clamp.

After carefully evaluating the concept designs, the decision was made to discontinue the development on static gravity balancers. The designs were considered too bulky to be used effectively at Hankamp Gears. Moreover, the range of motion of the static balancer would be insufficiency to cover the required movement for the gear loading scenario. It was therefore decided to develop a novel mobile lifting aid: an exoskeleton.

1.3 EXOSKELETONS

There are several options to support the employees at lifting operations. Most obvious would be a crane [22]. However, available cranes and forklifts are barely used at Hankamp Gears for payloads between 5 and 30 kg because they are not at immediately disposal and unsuitable to perform precise movements. Therefore exoskeletons could offer a solution. Exoskeletons are an exterior mechanism with the purpose of augmenting or assisting the human [19]. An exoskeleton could offer the employee full body support which is always at immediate disposal.

(a) (b) (c)

Figure 4: (a) Hardiman (*GE*). (b) BLEEX (*University of Berkeley*). (c) Esko GT (*Esko Bionic legs*).

The first attempt for an industrial exoskeleton dates back to 1965. GE built the Hardiman; a powered exoskeleton to enhance human strength. The machine, shown in Figure 4a, was able to lift 340 kg, however its own weight was massive 750 kg. In the last decades exoskeleton research was mainly driven by military funds. An example is the BLEEX, see Figure 4b which was funded by DARPA. This lower limp exoskeleton suit is designed to assist soldiers carrying load. Continuous improvements resulted in weight decrease and power increase. Currently, there is much interest in medical exoskeletons which could aid ambulatory impaired subjects, for example the Esko GT (shown in Figure 4c).

1.3.1 *Industrial exoskeletons*

Research showed that an exoskeleton could reduce work related injuries [10, 1, 41]. Most developed exoskeletons are designed for research in the area of either health care of military, but the interest for industrial exoskeletons is booming. In Appendix A an overview of industrial exoskeletons is presented, categorized in heavy duty, arm support and lumbar support. Most relevant competitors for this project are passive industrial body exoskeletons.

Four of those passive industrial body exoskeletons (see Figure 5) are discussed below. First, the Lockheed Fortis. This is a fully passive exoskeleton which utilizes a propitiatory gravity balancer. The exoskeleton is able to balance heavy tools up to 20 kg. Trunk support is provided by a counterweight. The Esko Work suit is very similar, but uses the ZeroG[1]. BEA systems developed the O-ArmX. The exoskeleton also contains arm supports from ZeroG, but in contrary to the above, contains a powered leg module. Trunk support is

1 The ZeroG is a commercial available arm support by Equipois.

provided by an 18 V battery which also serves as a counterweight. Last, Suitx MAX is an agile full body exoskeleton that reduces forces on the back shoulder and knee.

Mentioned exoskeletons offer a solution for for example handling heavy tools at prolonged overhead work in construction or automotive industries. However, they are designed for a static payload and are therefore unsuitable for pick and place operations.

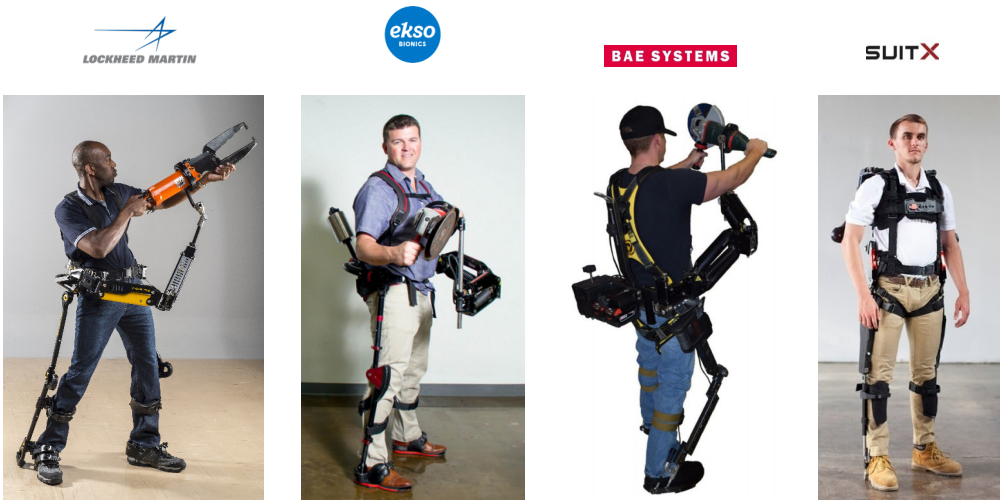

(a) (b) (c) (d)

Figure 5: Industrial full body exoskeletons. (a) Lockheed Fortis. (b) Ekso Works. (c) BEA Systems O-armX. (d) Suitx MAX.

1.3.2 *Patient Caring exoskeletons*

Patient carrying could be a physical demanding for nurses. Few researchers focussed on a solution for nurses. First the RIBA-II, developed by researchers at RIKEN and Tokai Rubber Industries, see Figure 6a. The robot can lift patients up to 80 kg. Another approach was explored by Yamamoto et al. [42]. The researchers developed a full body exoskeleton suit (see Figure 6b) where the human joints are assisted by pneumatic actuators.

The H-Haptics group in Delft focusses on a haptic clinical lifting aid. An impression of the Delft lifting aid solution is shown in Figure 6c. It contains a passive cart and two passive haptic arms. The requirements for the arm support are very similar to the industrial exoskeleton and therefore it was decided to develop the arm support for both the industrial as the clinical setting.

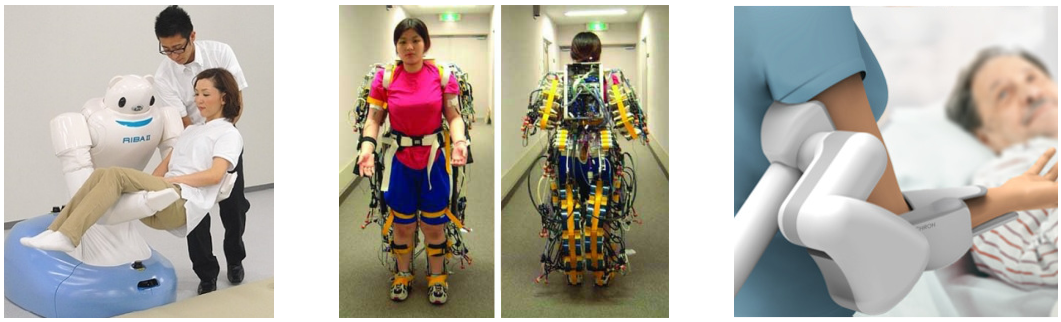

(a) (b) (c)

Figure 6: Devices developed for patient caring. (a) RIKEN Riba 2. (b) Power Assisting Suit [42]. (c) Impression of the Delft lifting cart.

1.4 OBJECTIVE PDENG

The goal of this assignment is to develop a wearable lifting aid for the machine operators at Hankamp Gears. Passive exoskeletons capable of this range of payloads are largely unexplored. Although it is assumed that an exoskeleton could increase productivity, this project is focussed on a solution to reduce injuries for employees performing pick and place operations. Moreover, with increasingly stringent norms and regulations the need for lifting devices is increasing.

1.4.1 *Stakeholders*

This project is a collaboration between industry and university. A list of the key stakeholders with their primary interest are presented in Table 1.

1.4.2 *User requirements*

User interviews are a powerful method to deduct the user desires for the lifting aid. In total four users were interviewed:

- *Freek Tonis* - CEO Hankamp Gears and CEO Hankamp Rehab,
- *Arvid Keemink* - PhD Candidate at the University at Twente,
- *Bart Rotting* - All round machine operator and coordinator at Hankamp Gears,
- *Boudewijn Wisse* - CEO Leavo.

The key user requirements deducted from the interviews are summed in Table 2.

Table 1: List of key stakeholders with the primary interests concerning the development of the lifting aid.

STAKEHOLDER	PRIMARY INTEREST
STW - Project Owner	Socio-economic aspects of the project.
UT - Professor	Advancement in exoskeletons.
UT - PhD Candidate	Theoretical haptic research.
UT - PDEng Candidate	Development of prototype(s) within specifications
TUD - PhD Candidate	Arm support which could be integrated in the mobile car support system.
Hankamp Gears - Operator grinding machine	Well applicable solution for manipulating gears.
Hankamp Gears - Director	Reduced number of work related injuries.
Laevo	Functioning of novel exoskeleton mechanisms, in particular the lumbar mechanism.
Siza	Lifting aid for supporting the nurse with patient carrying.

1.4.3 *System requirements.*

The user requirements are translated into system requirements. The importance of human factors are evident for an exoskeleton. Inherent to an exoskeleton are human body dimensions, i.e. anthropometric data. The exoskeleton should fit the vast majority of operators. This desire is captured in the requirement that the exoskeleton should fit for a population of P5 - P95[2]. The exoskeleton should be able to provide full body support for the operators while performing pick and place tasks. The compensation should be automatically adjusted within one second from 0 to 25 kg. The exoskeleton compensation should be passive and constant over the human arm range of motion. Donning and doffing should be shorter than 30 seconds. Furthermore, the exoskeleton should feature untethered usage for at least two hours and should support unhindered walking upto 1 m/s. Lastly, safety is paramount for robot-user interfaces. The operator's safety should be guaranteed by potential hazardous situations e.g. unintentional dropping the gear, falling or lithium fire.

1.5 OUTLINE

Chapter 2 describes the development of the an industrial for pick and place exoskeleton operations. Concepts for the arm interface, arm support, trunk support and leg support are presented. In Chapter 3 the development of the automatic gravity balancer is pre-

2 Data was taken from Dined. The population taken was Dutch adults 2004,aged 20 - 60, male and female.

Table 2: Key user requirements.

REQUIREMENT	DESCRIPTION
1. full body support	The exoskeleton should support heavy payloads
2. safe	Safety is paramount for human interaction. In particular with an exoskeleton where the user is attached to the robot.
3. comfortable	The user should be able to wear the exoskeleton for prolonged time without discomfort.
4. fast donning doffing	Quick to don and doff over existing gear.
5. intuitive	The suit should be easy to use without training.
6. modular	Separable arm, trunk and leg support modules.
7. adjustable	Fit a wide range of employees dimensions.
8. low profile	Follows the employees movements in tight spaces.
9. low-priced	Retail price far below current industrial exoskeletons.

sented, including a detailed description of the mechanical design, simulations and safety mechanism. The discussion and conclusion are given in Chapter 4.

2

WINGMAS EXOSKELETON

This chapter describes the developed exoskeleton for industrial usage. It covers the design choices of the five different modules and describes various built proof of principles (POCs). The chapter concludes with the completely assembled exoskeleton.

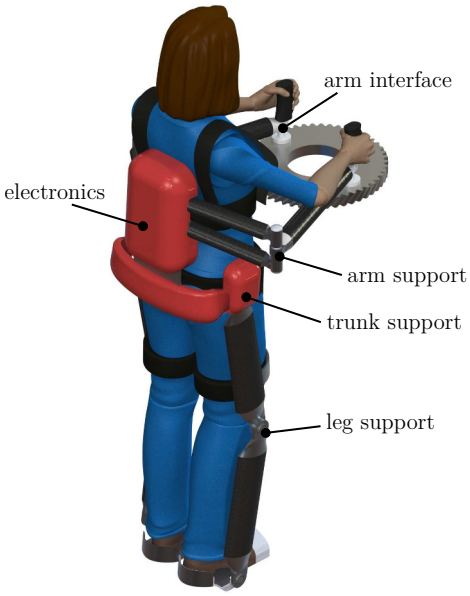

Figure 7: Modules of the exoskeleton.

The exoskeleton is subdivided into five modules, see Figure 7. The support constitute of a *leg* -, *trunk* - and *trunk support*. The *hand interface* is a separate module containing the end effector. The last module contains auxiliary *electronics*.

2.1 LEG SUPPORT MODULE

The leg support module function is to transfer the forces from the payload to the ground. The leg exoskeleton should be anthropometric and because loading the gear grinder machine is a dynamic task it should not impede walking. Three POCs were built to explore the possibilities for leg support (see Figure 8):

(a) (b) (c)

Figure 8: Leg support module POCs. (a) No parallelogram. (b) Upper leg parallelogram. (c) Upper and lower leg parallelogram.

- *No parallelogram*
  First, leg support with single rods, which is effectively similar to the Lockheed Fortis and Ekso Works. The mobility with this leg exoskeleton is almost unimpeded.
- *Upper leg parallelogram*
  This version contains an upper leg parallelogram and a single rod lower leg parallelogram. Walking was considered almost impossible because it was not possible to flex the ankle.
- *Upper and lower leg parallelogram*
  The current version of leg exoskeleton contains both upper and lower leg parallelograms. The ROM for walking was not interfered, however the exoskeleton impeded normal walking. This parallelogram is also discussed at the trunk module.

Note that with all the mentioned leg support concepts the perceived compensation is dependent on the stance. The leg is fully supported at straight stance, however decreases at ankle or knee flextion. The free body diagram of the leg parallelogram is presented in Appendix B.

2.2 TRUNK MODULE

Most reported complications due to lifting at work are related with lower back pain and therefore most research focussed on lower back pain, e.g. [31, 2, 39, 7, 38]. Four different methods of trunk support were evaluated (see Figure 9 for built POCs):

(a) (b) (c)

Figure 9: POCs thrunk support. (a) Counterweight, evaluated in [20]. (b) Spring, evaluated in [20]. (c) Paralellogram, evaluated in [35].

- *Counterweight*
  First, by means of a counterweight, 12 kg at 0.27 m and 6 kg at 0.54 m. This method affects the base of support, positively when handling payload but negatively at normal stance. The counterweight adds considerably to the exoskeleton total weight, making movements such as walking cumbersome.

- *Spring*
  The second method was by means of a spring element which provides an opposing moment around the hip. The Laevo was placed under the WingMAS but it quickly became clear that the Laevo does not provide the required compensation for this exoskeleton: support increases by hip angle and thereby the Laevo provides almost no support at stance. A custom spring trunk support was made which provides support at stance. Unfortunately, spring trunk supports hampers walking. The counterweight and spring were compared in a trial experiment with 12 subjects by Macke [20]. EMG measurements showed no significant difference between both methods. The NASA TLX [16, 13] questionnaire showed a preference for the spring mechanism.

- *Parallelogram*
  Both methods have disadvantages as described, but in addition, these methods also need active adjustment to compensate for dynamic trunk load. Therefore, a

third option was devised: a parallelogram. Rigid bars form a parallelogram which supports both the vertical force as the moment posed by the payloads gravity. During walking always one side of the parallelogram is connected with the ground. A first evaluation, by Velu, showed that the parallelogram was indeed able to counteract the moment and gravitation forces posed by the payload [35]. Nonetheless, a reaction force at the knee is required (increasing with knee flexion) and stiffness limited the conceived functioning of the parallelogram. The benefits of the parallelogram still outweigh the counterweight and spring and it was therefore decided to integrate an upgraded version of parallelogram into the WingMAS.

- *Fixation*
  Lastly, trunk support could obtained by fixating the human back. Obviously, this impedes trunk motions which reduces comfortably as well as obstructing required movements to load the gear grinder machine.

2.3 ARM SUPPORT MODULE

This section describes the working principles for the gravity balancer, mechanisms for energy-free adjustment and kinematics.

2.3.1 *Gravity balancer principle*

A gravity balance mechanism is used for the arm compensation. This mechanism, shown in Figure 10, is a passive mechanism and compensates gravity independent of the angle (ψ). The payload could be movable in 3D space and perceived as weightless. Gravity balancers has been widely used in arm supports [14, 25, 30, 34]. The free body diagram of the gravity balancer is presented in Appendix B. This chapter considers the Seabo MiniMAS as gravity balancer for the arm support. During this project a completely new gravity balancer was developed, to which Chapter 3 is devoted.

The working principle could be verified by conservation of energy. The total energy (U_t) in the gravity balancer is described by the potential energy of the spring (U_s) and potential energy (U_m):

$$U_t = U_s + U_m \tag{1}$$

The spring length (s) can be found with the cosine rule:

$$s^2 = a^2 + r^2 - 2\,a\,r\,\sin(\psi) \tag{2}$$

Where a represents the spring attachment position on the leadscrew, r the spring attachment position on the gravity balancer arm and ψ the gravity balancer angle. For an ideal spring the energy yields:

$$U_s = \frac{1}{2}\,k\,s^2 = \frac{1}{2}\,k(a^2 + r^2 - 2\,a\,r\,\sin(\psi)) \tag{3}$$

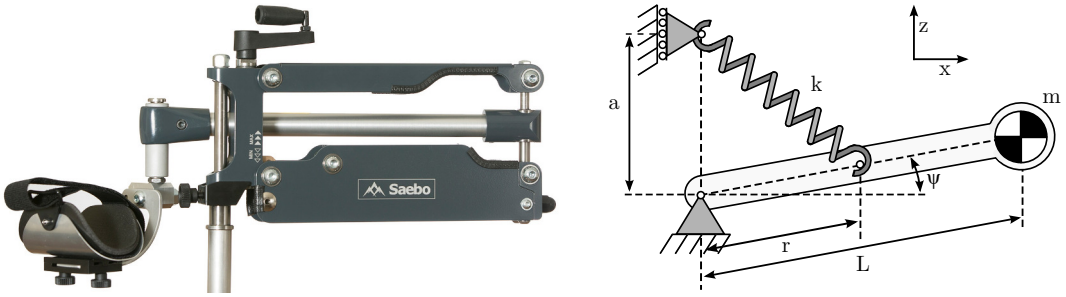

(a) (b)

Figure 10: (a) Seabo MiniMAS: commercial available gravity balancer (arm support) for stroke patients. (b) Schematic of the gravity balancer.

The potential energy is:

$$U_m = m\,g\,L\sin(\psi) \tag{4}$$

Where L is the gravity balancer arm length and g is the gravitational constant. The moment around the pivot point can be found by differentiating to ψ:

$$\frac{\delta U_t}{\delta \psi} = \cos(\psi)\,(m\,g\,L - a\,k\,r) = 0 \tag{5}$$

The mass is perfectly balanced if:

$$a\,k\,r = m\,g\,L \tag{6}$$

This equation shows that the compensation could be adjusted by changing the spring attachment height (a), which is a linear relationship.

2.3.2 *Energy-free adjustment*

Manual adjustment of the traditional gravity balancer could be cumbersome. Most notability increasing the compensation, where energy has to be inserted into the system. Several mechanisms has been devised that can adjust the compensation of the gravity balancer *energy-free*, see Figure 11:

- *Virtual spring concept* [40].
  This mechanism contains two springs which results, by superposition, to one virtual spring. By attaching both springs on a predefined circle, one is able to adjust the springs without changing their length. Thereby, the adjustment is energy-free.
- *Simultaneous displacement* [33].
  By changing both the spring attachment points (a and r) simultaneously, one can alter the compensation without changing the spring length.

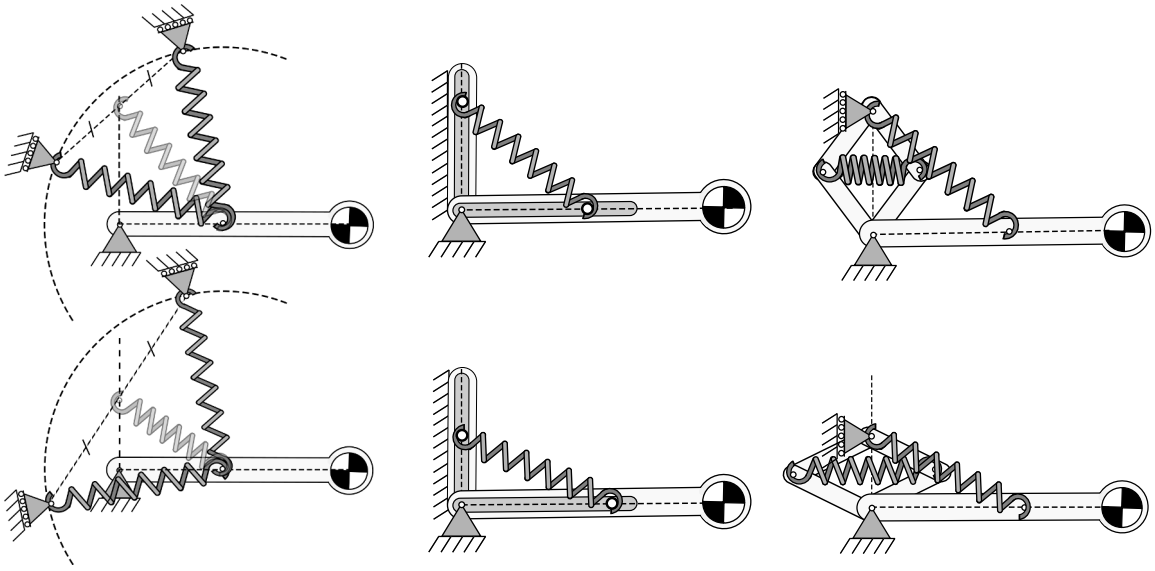

(a) (b) (c)

Figure 11: Energy free adjustment mechanisms from literatue. (a) Virtual spring concept [40]. (b) Simultaneous displacement [33]. (c) Spring-to-spring balancing [5].

- *Spring-to-spring balancing* [5].
  An additional spring can be added to store energy.

All concepts require the adjustment to be at a predetermined angle. This is required to suffice the law of energy conservation. When adjustment would be performed at a different angle, the total energy in the system would change. It would therefore be impossible to pick up a payload at a lower position than it would be placed, as potential energy is gained. For that reason it is required to insert energy into the system. In Appendix E two concepts are presented which describe a mechanism with a secondary spring (similar to the spring-to-spring balancer) where energy is stored with the purpose of extremely fast adjustments. Unfortunately, the effectiveness of the secondary spring is limited due to added friction on the leadscrew. Moreover, the secondary spring greatly increase complexity. It was therefore decided to not use a secondary spring.

2.3.3 *Kinematic configurations*

Two gravity balancers have to be mounted on the exoskeleton. Various configurations could be devised, the two most practical are shown in Figure 12. The configuration with the gravity balancer as robotic upper arm and a horizontal link as robotic lower arm has been chosen because it contains fewer links (which decreases complexity and weight). The location of the gravity balancer attachment on the exoskeleton and the lengths of

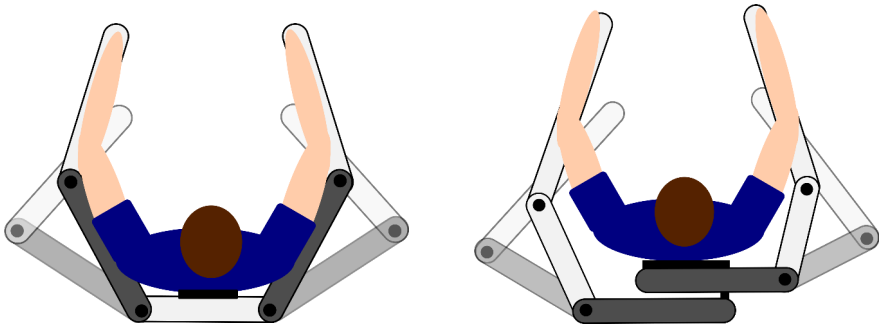

(a) (b)

Figure 12: Two possible kinematic robot arm configurations. Horizontal links are shown in white and the gravity balancer is shown in gray. (a) Gravity balancer is able to rotate. (b) Gravity balancer fixated to the back, ROM is provided by two planar links.

the parallelogram and horizontal links were optimized to the gear grinder at Hankamp Gears (Reishauer RZ400), shown in Figure 13. The optimized gravity balancer locations with respect to the human shoulder are p_x = 0.1 m, p_y = - 0.05 m and the gravity balancer parallelogram length L_1 = 0.4 m and horizontal link length L_2 = 0.5 m.

2.4 HAND INTERFACE MODULE

The end effector of the exoskeleton should be attached to the payload and should be manoeuvrable by the human. In other words, a physical connection between the exoskeleton and the human has to be made. Concepts for a gimbal, robot-human interface and sensor type are described below.

2.4.1 *Degrees of freedom*

The end effector of the Seabo-MiniMAS could be equipped with a standard arm cuff or a gimbal, with respectively 4 DOF (three translational and one rotational) and 6 DOF. The rotational axis of the MiniMAS gimbal arm cuff are however not aligned with the upper arm rotational axis. Therefore, arm rotation induces tedious translations of the arm cuff.

A novel end effector, shown in Figure 14a, was designed where the axes of rotation are aligned with the human axis of rotation. This end effector had three rotational DOF (the three translational DOF are facilitated by the gravity balancer). Moreover, the concept includes a second gravity balancer to compensate elbow flexion.

It was decided to not add a second gravity balancer to the arm support since it would greatly enhance complexity (i.e. the gravity balancer should contain an automatic adjustment mechanism) and increase (end point) weight. In Figure 14b a physical POC

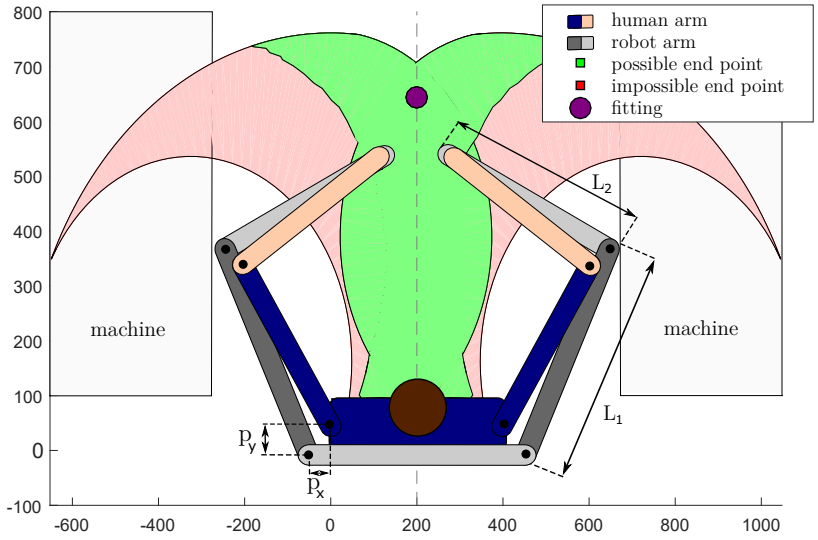

Figure 13: Range of motion of WingMAS when inserting the gear onto the gear grinder fitting. Range of motion with and without collision with the gear grinder are shown in red and green respectively. The location of the gravity balancer with respect to the human elbow is addressed with p_x and p_y. L_1 and L_2 represents respectively the length of the gravity balancer parallelogram and the horizontal link.

is shown without the second gravity balancer. This arm cuff is statically balanced by a counterweight.

2.4.2 *Human-Robot interface type*

Human-robot interfaces were evaluate by Schorsch and Abbink [28]. Three arm interface attachment types could be distinguished (see Figure 15):

- *Anthropocentric*
  The human is in direct connect with the payload and supported from the robot goes through the human. The researchers found that anthropocentric lifting is advantageous for fast movements in lifting.

- *Robocentric*
  The robot is in direct contact with the payload and the human is steering the robot.

- *Hybrid*
  Combination of both anthropocentric as robocentric interface. The support is almost entirely provided by the robot but the human is still in contact with the gear which enhances the feeling of control.

(a) (b)

Figure 14: Gimbal designed for the arm interface. The rotation axes are indicated as arrows. (a) CAD design with spring compensation. (b) POC with counterweight for static balance without payload.

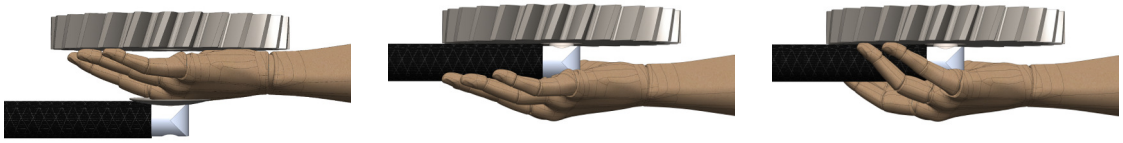

(a) (b) (c)

Figure 15: Human-robot hand interface types. (a) Antropocentric. (b) Robocentric. (c) Hybrid.

2.4.3 *Arm interface sensor type*

The AGB balancer should be able to adjust compensation according to a giving input, by means of a sensor. In essence, the applicable sensors could be divided into three categories:

- *Manual*
  A potentiometer (either linear of rotary), or keypad, determines a value proportional to the compensation level. This provides the user manual control over the compensation level.

- *Threshold*
  At Hankamp Gears employees typically complete a batch of gears with the same known weight. Therefore, pick and place tasks could be executed by a binary signal from a push button where the compensation level is predefined. The push-button could be manually triggered by a remote control or in a gripper where the push-button is located between the gripper and the payload. The push-button could be

Figure 16: POCs hand interfaces. (a) Gloves with integrated FSRs. (b) Hybrid gripper with load cell. (c) Electro magnetic gripper with on/off button.

replaced by FSRs (with a threshold value) in gloves for an almost anthropocentric experience: the device will switch to compensation mode as soon as an object is grasped).

- *Load estimation*
  The device measures the weight and proportionally controls the gravity compensation *continuously*. This is inherently an unstable positive feedback method that could function properly when moving in 'free air' but can become dangerous when the gear is obstructed.

Several hand interface POCs have been built, three are shown in Figure 17. First, a 3D printed hybrid gripper was made where the payload could be measured by load cell. Another option is weight estimation or detection by gloves with integrated FSRs.. Picking up stacked gears could be difficult when approaching the gear from bellow. Electromagnets offer a solution because the gripper can grab the gears from above. A load cell could easily be implemented with this robocentric solution.

The latter concept is elaborated, see Figure 17a. The gripper contains three adjustable links (*RAM-B-201U-C Long, RAM Mounts*) which form a tripod configuration, able to adjust to gears ranging from 100 mm to 300 mm. The gripper contains three mechanical switchable clamp magnets (*Magjig 95, Magswitch*) which are able to hold 105 kg each. The concept for the gripper (see Figure 16a) is equipped with remote controls for increased (up) and decreased (down) compensation and on/off button to engage the electromagnets.

Another solution is to place the load cells under the shoes (not shown). This is deemed complicated and expensive, since additional information from IMUs is required to compensate for the user's posture and accelerations.

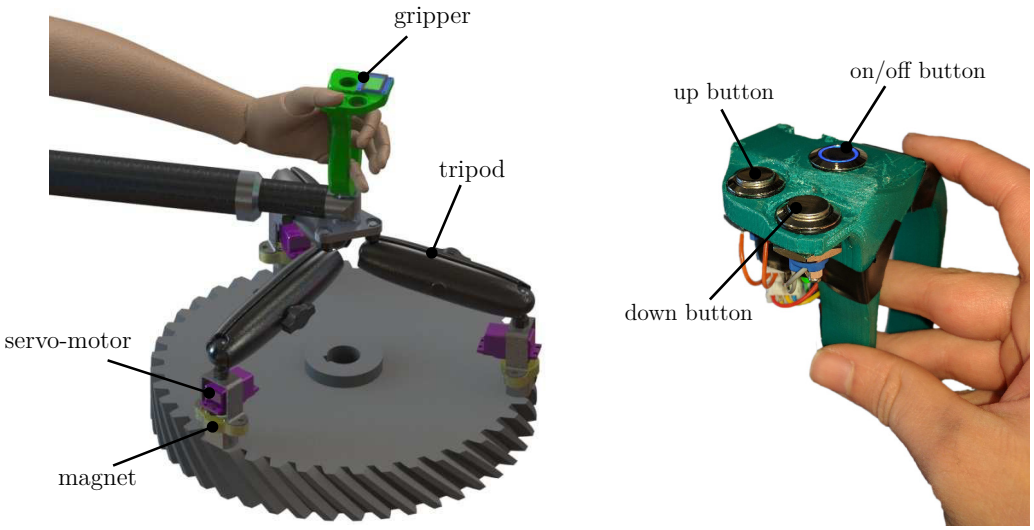

(a) (b)

Figure 17: (a) CAD design of the tripod magnetic gripper. (b) Remote controller with up and down buttons and on/off button.

2.5 ELECTRONICS MODULE

One of the requirements state that the exoskeleton should be semi-(passive). Nonetheless, electronics are required to adjust the arm compensation to the payload. The exoskeleton should be able to operate untethered. This implies that the exoskeleton should be self-powered and thus containing batteries. Key electronic elements that should be incorporated into this module are shown in Figure 18[1].

2.6 EXOSKELETON PROOF OF CONCEPT

The first version of the WingMAS, shown in Figure 19a, was built in an early stage of the project. This prototype contained the Seabo MiniMAS arm support, single rods leg support and a back plate which fixates the trunk. The POC was fully passive, i.e. it did not include electronics. The Seabo MiniMAS is only able to support 5 kg per arm, in contrast to the desired 25 kg per arm. Nonetheless, this POC provided valuable insights.

The weight of the payload is nicely transferred to ground. Subjects immediately perceived the alleviation of the payload. This effect was less pronounced when reaching out due to increased moment and lack of trunk support.

One of the greatest disadvantage of the WingMAS is impeded movement. Therefore, a concept for a second version WingMAS was devised. The second version, see Figure 19b,

1 The shown electronic components are used for the novel gravity balancer and are presented in Appendix D.

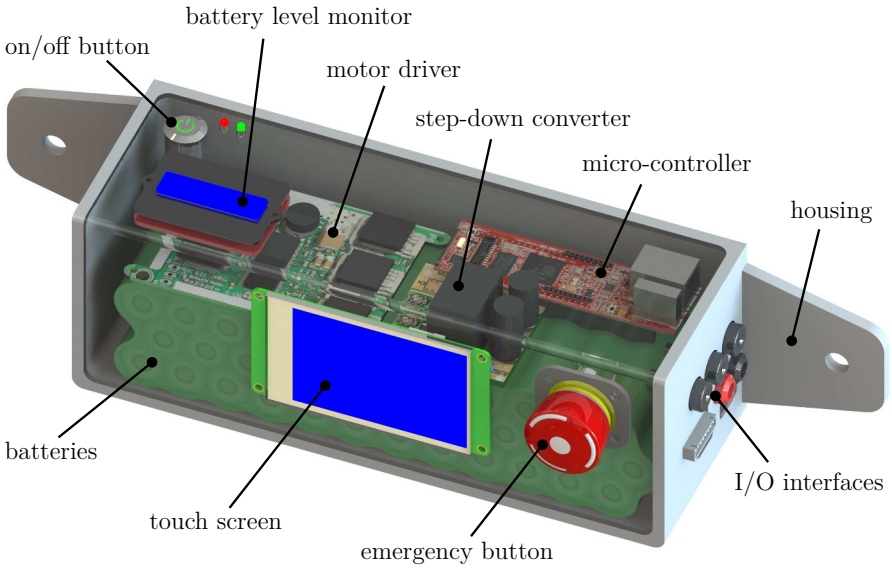

Figure 18: CAD design electronics module.

greatly enhanced mobility by omitting the back plate. The arm support modules were directly attached to the leg module close to the hip. This design also decreases donning and doffing time because there are merely attachments to the human at the foot, shin and hip.

(a) (b)

Figure 19: WingMAS exoskeleton. (a) First version. (b) Concept second version.

3 AUTOMATED GRAVITY BALANCER

In this chapter the novel arm support is presented: the Automatic Gravity Balancer (AGB). The devised mechanical design is discussed, e.g. the spring and leadscrew selection and compensation offset due to pulleys are discussed. Furthermore, a POC for automatic adjustment and the implemented safety mechanism are presented.

3.1 AUTOMATIC COMPENSATION ADJUSTMENT

The WingMAS contained a fully passive gravity balancer. It is a requiste to add an actuator in order to adjust the compestion automatically instead of mannually. Automatic adjustment of the gravity equilbartor has been described in lituature in [4, 21].

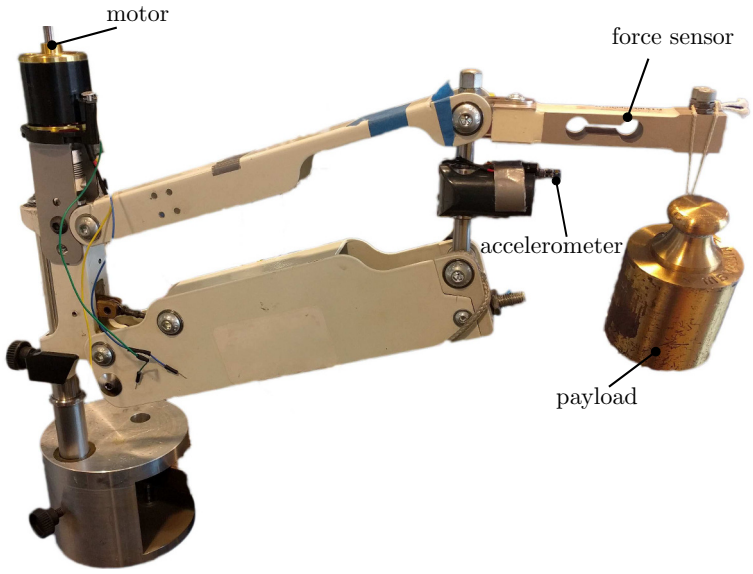

Figure 20: POC of the automatic adjustment mechanism (second versions).

3.1.1 *Proof of concept*

Two POCs for the automatic gravity balancer were built. A Seabo MiniMAS was used as the gravity balancer. An overview of the used electrical components of both POCs are presented in Appendix D.

The first version contained a brushed DC motor (*148867, Maxon*) with an encoder (*225787, Maxon*). Compensation adjustments were performed by rotating the leadscrew, where the leadscrew nut determines the spring attachment height (a). Feedback was obtained by an integrated linear potentiometer attached to the leadscrew. The setup was equipped with a force sensor (*CZL635, UCHI*) and amplifier (*SG 3016, ICP DAS*). Furthermore, a H-bridge (*18v25 CS, Pololu*), Arduino Mega and LiPo battery (*Nano-tech 2650mah 6S, Turnigy*) were used. This first setup successfully demonstrated possibilities for automatic adjustment for a gravity balancer. However, adjustments were too slow (in the order of seconds). It was therefore decided to alter the setup.

The major alteration of the second version was the choice for a more powerful motor. The DC motor was replaced with an outrunner (*SII 4035 250, Scorpion*), attached to a brushless driver (*Hobbyking X-CAR 120A, Hobbying*). Moverover, an accelerometer (*MPU 6050, Invensense*) was added to facilite payload estimation during movements. The second version of the POC AGB is shown in Figure 20 and was evaluated by Schneider [27]. Although use of a combined load cell and accelerometer resulted in a dynamic payload estimation, it was chosen to merely use a load cell for simplicity reasons.

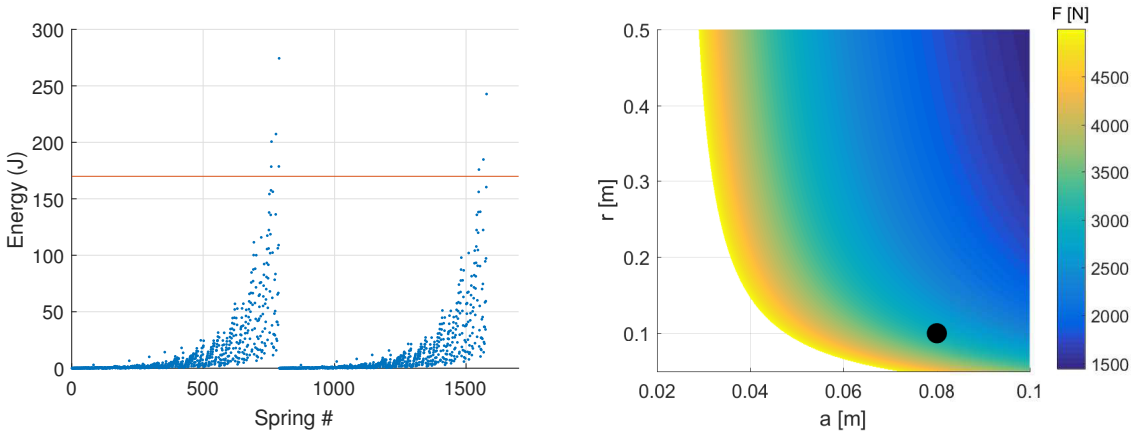

(a) (b)

Figure 21: Cable tension as a function of the gravity balancer parameters r and a. Cable tension above 5000 N has been disregarded. For the AGB an $a = 0.08$ and $r = 0.1$ and was chosen, indicted with the black dot.

3.2 MECHANICAL DESIGN

Initially it was intended to upgrade the MiniMAS's design to 25 kg, however major design changes had to be made and therefore it was decided design a new arm support from scratch. The draft design of the AGB was made by Koen Heuver. The mechanical design

of the AGB contains besides the elementary components an actuator and accompanied drivetrain.

3.2.1 *Spring selection*

Arguably the most important element in the AGB is the spring. The spring serves as an energy storage allowing for infinite motion without the requisite of inserting external energy, when the payload is constant. Traditionally, gravity balancers contain a helix coil spring. In Appendix C it is shown that a tension gas spring could also be successfully used in the gravity balancer. Gas springs typically have larger spring constant (k) and a more compact form factor than a helix coil spring.

It was attempted to utilise commercial off-the-shelf springs. In Figure 21a an overview of available Tevema[1] tension springs is presented. The plot shows that most springs could not store the required energy, while the few that could store the energy are unsuitable for their large dimensions. Therefore it was decided to use a spring with custom parameters: wire diameter (d), coil diameter (D) and spring length.

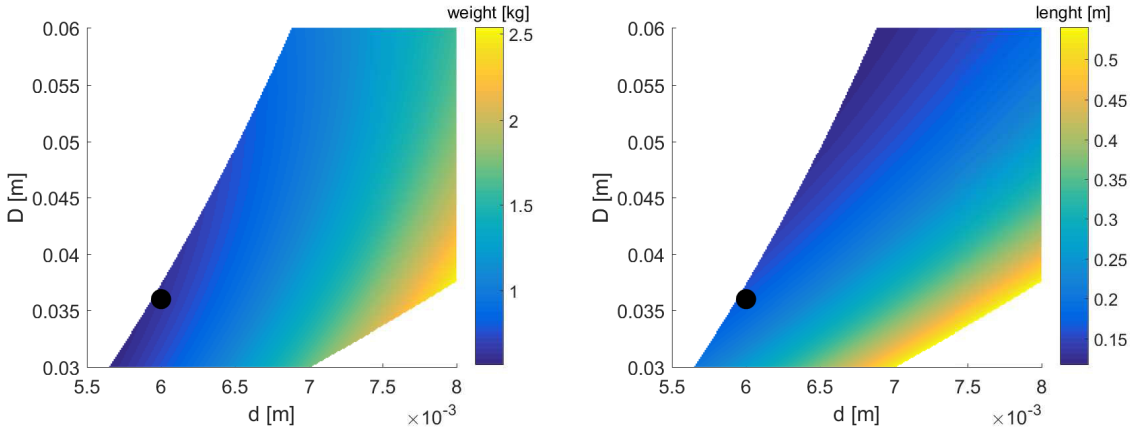

(a) (b)

Figure 22: Custom springs parameter evaluation. On the horizontal axis the wire diameter (d) and on the vertical axis is the coil diameter (D) diameters. Springs that could not handle the payload are disregarded. The black dot indicates the chosen parameters $d = 0.06$ and $D = 0.036$. (a) Spring weight. (b) Spring length.

First, the desired stiffness had to be determined. The stiffness of the spring could be determined with the gravity balancer equation $a\,k\,r = m\,g\,L$. The right hand side of the equation are predetermined values, which leaves r and a as the design parameters. The plot Figure 21b shows suitable r and a values. It is desired to have the cable tension as

1 Tevema is a major spring seller and served as a reference for commercial available off-the-shelf tension springs.

low as possible in order to minimize the required motor torque. The values $r = 0.1$ m and $a = 0.08$ m were chosen, which resulted in a spring stiffness of 2697.8 N/m.

A variety of custom springs can be made with the same predetermined stiffness. In Figure 22 the weight and length of customs springs are shown as a function of wire diameter (d) and coil diameter (D). Unfortunately, there was no suitable solution for a single spring, however two springs in series provided a feasible solution:

	stiffness (N/m)	d (m)	D (m)	L_k (m)	L_0 (m)
spring 1	4046.6	0.06	0.036	0.064	0.1074
spring 2	2023.3	0.06	0.036	0.171	0.215

Where L_k and L_0 represent the initial coil length and total spring length respectively.

3.2.2 *Cable configuration*

The previously discussed gravity balancer considered ideal springs, i.e. zero-free length. By cautiously determining the pretension, the spring could behave as zero-free length. Commonly, a cable is used in gravity balancers to relocate the spring. Another approach was used by Altenburger et al.. The researchers added an extra linkage to the spring attachment which resulted in almost ideal spring behaviour [3].

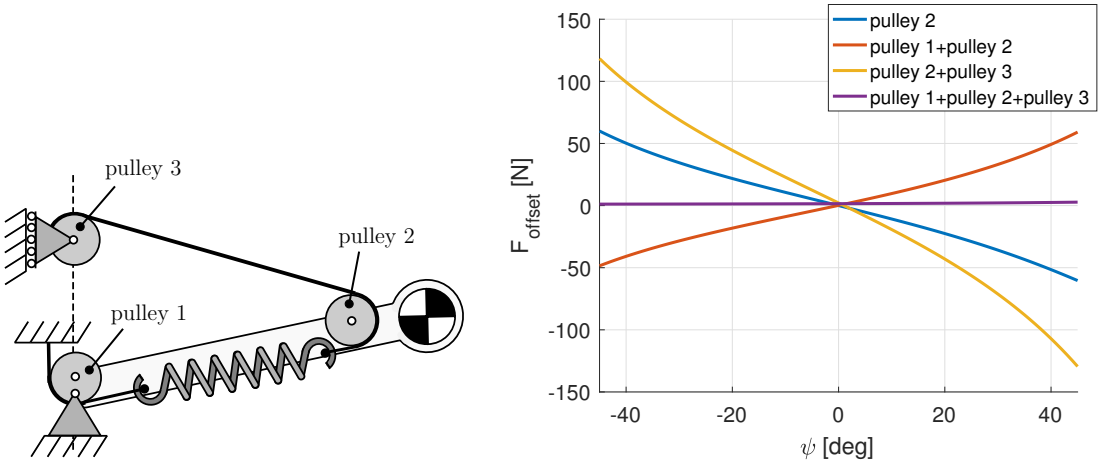

(a) (b)

Figure 23: Gravity balancer equipped with multiple pulleys. (a) Schematic with three pulleys. (b) Erroneous compensation force due to pulley(s).

The cable is guided by one or more pulleys. By incorporating three pulleys (see Figure 23a) the circumference of the cable guided on the pulleys exactly adds to $2 \cdot \pi \cdot r$, which does not results in a compensation offset dependent on ψ. Therefore, this pulley setup has the preference. The first mechanical CAD design of the AGB included three pulleys, however the design became too complex (in particular the alignment of the pulley 1 and pulley 3 at zero compensation, $a = 0$).Therefore, an attempt was made to design the AGB with less pulleys.

The compensation offset as a function of ψ of various pulley configurations is shown in Figure 23. These plots show large compensation errors. It was therefore decided to evaluate the compensation error with cable guidance similar as in the Saebo MiniMAS. In Figure 24 it can be seen that the erroneous offset due to the cable guidance under the pulley is very low. Therefore it was decided to use this pulley setup. The cable tension is a function of a and ψ, shown in Figure 25a. The maximum cable tension is 2245 N.

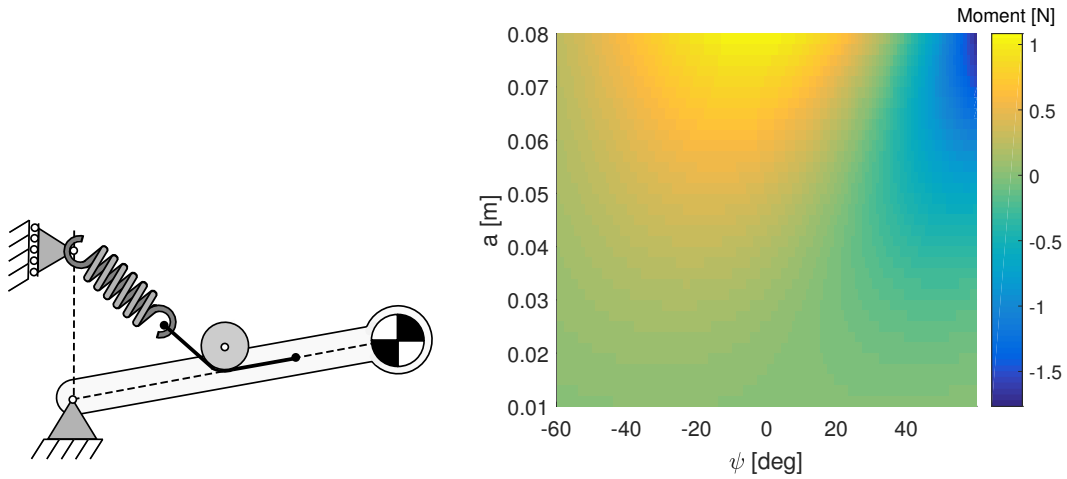

(a) (b)

Figure 24: Gravity balancer with the cable guided under one pulley. (a) Schematic. (b) Erroneous compensation force due to the pulley.

3.2.3 *Leadscrew*

An essential component for the adjustment of compensation is the leadscrew. The vertical and horizontal forces on the leadscrew nut are:

$$F_z = -a\,k + r\,k\,\sin(\psi) \tag{7}$$

$$F_x = r\,k\,\cos(\psi) \tag{8}$$

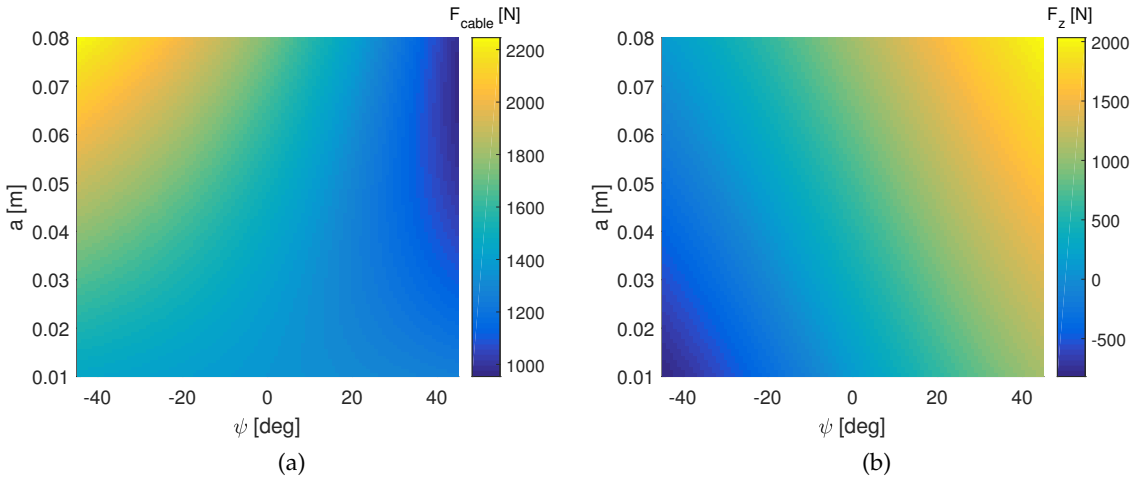

Figure 25: (a) Cable tension as a function of a and ψ. (b) Vertical force on leadscrew as a function of a and ψ.

As shown in Figure 25b, the vertical force on the leadscrew can be both positive as negative. The leadscrew induces high friction, which is dependent on the force on the leadscrew nut, pitch angle and friction coefficient. It is desired to decrease the friction to the limit of self-lockness (0.5 efficiency). Different commercial available leadscrews were considered, see Figure 26. The coefficient of friction was estimated to be 0.12 (based on a greased bronze nut and steel leadscrew). The selected leadscrew is *TR12x3*.

3.2.4 *Design AGB assembly*

The mechanical design of the AGB is presented in Figure 27. The AGB is designed with a Factor of Safety (FOS) of 1.5. The horizontal arm is made of a carbon fiber telescopic tube, which is able to adjust in length from 285 to 464 mm.

The cable and spring configuration are shown in Figure 28. The spring is pretensioned by a screw located on the distal end of the parallelogram. The design features a tapered bottom U profile which allows for a compact design. The DOF are measured with sensors, numbered in the figure. The corresponding ROM are respectively 360 deg (limited by cables), 120 deg and 230 deg.

A detailed view of the drivetrain is shown in Figure 29a. It contains a timing belt (*HTD5M 15 mm*) with a gear ratio of 2.

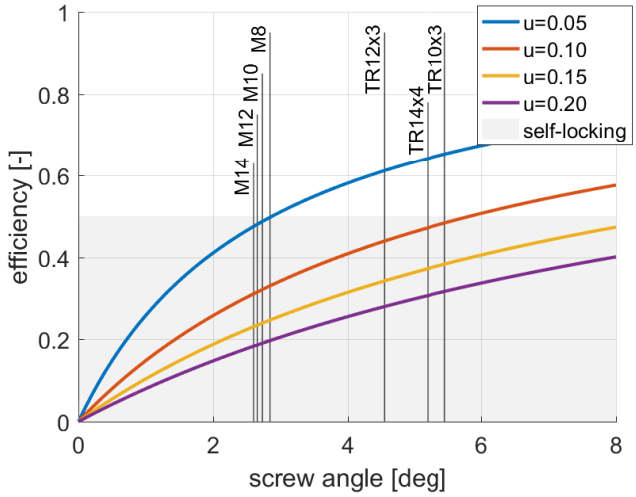

Figure 26: Commercial available leadscrew pitch angles versus efficiency. The grey area indicates 'self-lockness'.

3.3 ELECTRONICS AND CONTROL ARCHITECTURE

3.3.1 *Electronic components*

The electrical components are similar to the POC for the automatic adjustment mechanism, although more powerful due the higher payload demand. Brushless outrunner motors offer excellent power to weight ratios. Simulations with various outrunners were performed and (*Motor 6374, DIY Electric Skateboard*) was chosen. The motor requires a powerful brushless driver (*VESC, DIY Electric Skateboard*). The driver could be used sensored and sensorless. Both a hall sensor as an encoder (*HEDM-5540-B13, Broadcom*) could be used. An 18600 battery pack, in a 12S3P configuration, with a Battery Management System (BMS) (*12S3P Samsung 25R, Energus*) was chosen as the energy supply. The payload is estimated with a 50 kg load cell (*TAS606, HTC-sensor*) and the MBED controller (*LPC4088, Embedded Artist*) was used as the microcontroller. The AGB is equipped with three encoders (*AS5048, AMS*) which measure the AGB DOFs (see Figure 28). An overview of the used electronics are presented in Appendix D. Two proto shields were built with JST-XHP 2.54 connectors, see Appendix G for the *EA LPC4088* and *Arduino Mega* shield respectively. Furthermore, the AGB could be interfaced with a GUI. Preliminary tests have been performed with a TFT touch display (*NX4832T035, Nextion*), see Figure 30).

The performance of the drivetrain was simulated to verify its capabilities. The simulation model and simulation results are presented in Appendix F.

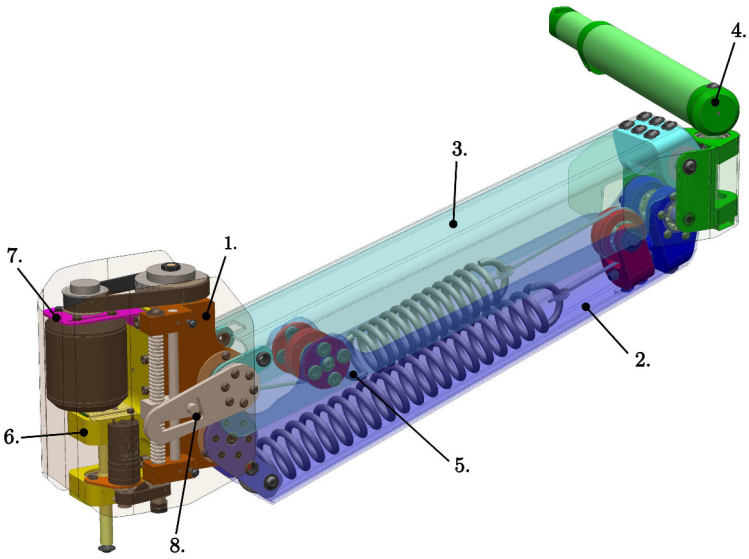

	SUB-ASSEMBLY
1.	compensation adjustment
2.	bottom U profile
3.	upper U profile
4.	horizontal arm
5.	spring and cabling
6.	hip attachment
7.	motor attachment
8.	safety mechanism

Figure 27: CAD design of the arm module with sub-assembly annotation.

3.4 CONTROL ARCHITECTURE

Various hand interfaces were described in Section 2.4. It was chosen to maintain versatility and implement multiple control methods for the AGB:

1.	slider	The compensation level is set proportionally with an analogue slider.
2.	buttons	Two button, an up and a down button to increase and decrease the compensation level respectively.
3.	FSR threshold	Two FSRs (force sensitive resistors) are integrated into a glove. A threshold is set to distinguish the no payload and a payload. The compensation level is set by a slider.
4.	FSR proportional	Utilises the same FSRs but alters the compensation proportional the payload measured at the gloves.
5.	load cell	Similar to the FSR proportion method but with a load cell for more accurate measurement.
6.	serial input	Compensation level is set by communicating the desired compensation via UART.

There are two safety levels incorporated for the automatic adjustment. The first safety level consist of software end stops, set to 15% and 85% of the range of the potentiometer. The second level are physical ends stops, positioned at 7% and 93%. The end stops and potentiometer are integrated in the AGB adjustment unit as shown in Figure 27.

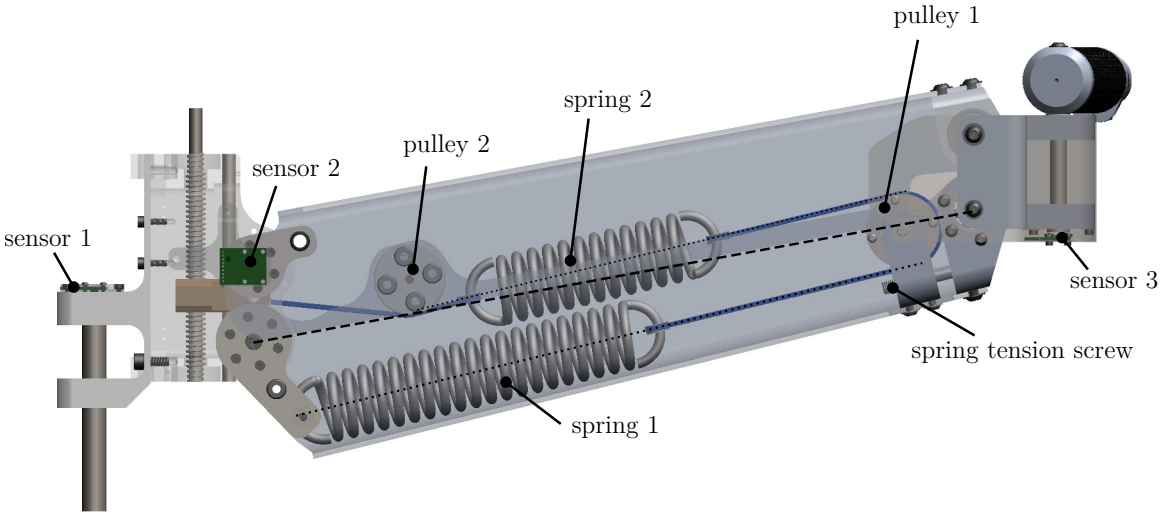

Figure 28: AGB spring configuration. The bottom U profile is slightly tapered (angle between the dotted and dashed lines). The AGB is equipped with three encoders to measure the kinematics.

3.5 SAFETY MECHANISM

The spring energy in the arm could potentially cause unsafe situations, in particular when the payload is suddenly released. The devised solution entails a dynamic end stop. Two concepts are shown in Figure 31, a rotary and a linear variant. The mechanism is composed of a slot and an actuated pin which follows the arm at a restricted angular velocity. The pin has a restricted range of motion in the slot, which results in a constrained end effector movement of the AGB. The movement of slot is facilitated by an electromotor. An important feature is the self-locking mechanism, e.g. a worm gear or leadscrew, which ensures that the safety mechanism is not backdrivable.

3.5.1 *Rotary dynamic end stop*

The rotary variant contains an arced slot. An encoder measures the error (e), which is the difference between the pin and motor angle. Subsequently, the actuator is controlled with a constrained angular velocity. A POC was built for the rotary safety mechanism, shown in Figure 32a. This setup successfully verified proper function of this mechanism.

3.5.2 *Linear dynamic end stop*

Unfortunately, the worm gear would be too heavy to be implemented in the AGB (should be able to withstand 230 Nm) and therefore it was decided to integrate the linear dynamic

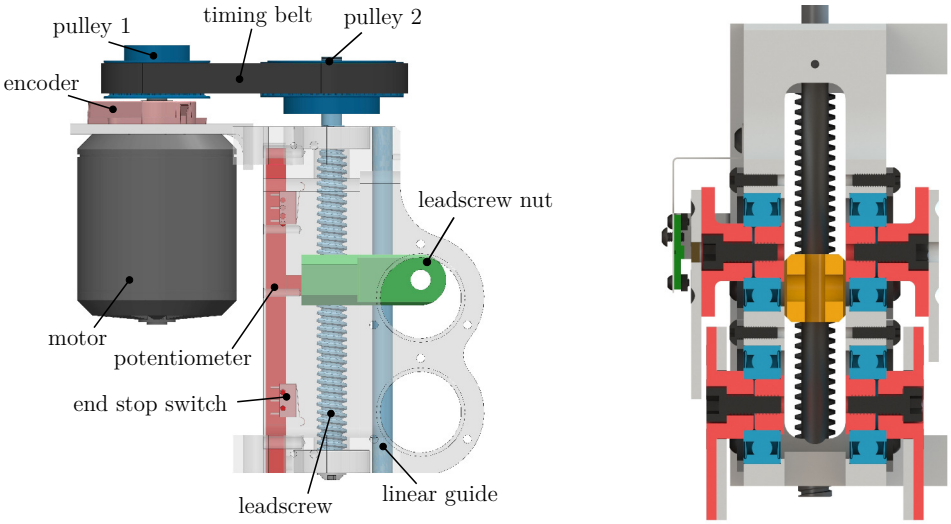

Figure 29: AGB detailed views. (a) Drivetrain. (b) Section view adjustment unit.

safety mechanism. The design is much slimmer and lighter and could therefore be discretely integrated into the AGB design (see Figure 27). The leadscrew (*TR12x3*) and DC motor (*25Dx48L mm GR4, Pololu*) are connected with a timing belt.

The arced slot of the rotary end stop results in an equal allowed unimpeded end point movement for positive as negative AGB angles. Unfortunately, this is not possible with the linear variant. The shape of the slot is different with a positive ψ than with a negative ψ, denoted with respectively + and -. The shape of the upper and lower bounds are calculated with:

$$[x_+, y_+] = \left[\frac{d}{\cos(\psi)} + r\,\sin(\psi), r\,\cos(\psi)\right] \tag{9}$$

$$[x_-, y_-] = \left[\frac{d}{\cos(\psi)} - r\,\sin(\psi), r\,\cos(\psi)\right] \tag{10}$$

Where d represents the desired vertical end point movement before the end stop is hit. The calculated bounds are shown in Figure 32b. A possible solution is a first order fit between the upper and lower bound.

The dynamic end stop has numerous advantages over conventional safety mechanisms (e.g. a static end stop or a disk brake). First and foremost, this mechanism is fail safe. Even with a malfunctioning motor the system remains safe. A power cut results in a stationary pin, effectively limiting the range of motion. Furthermore, an erroneous motor actuation does not result in an unsafe situations because the motor is not strong enough to overcome

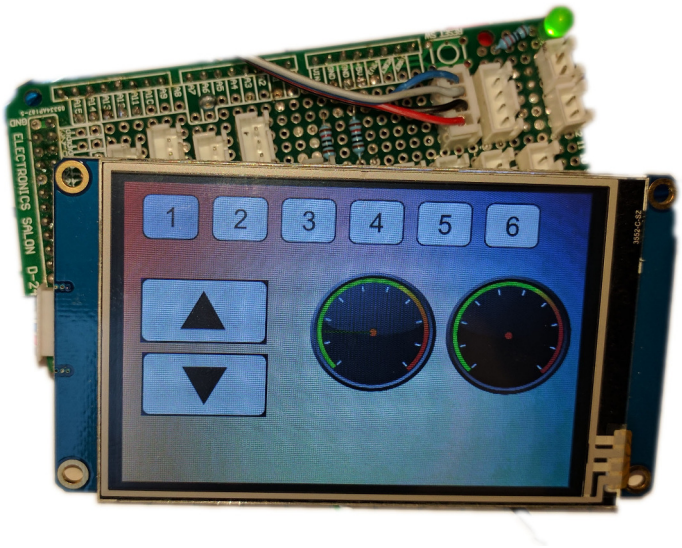

Figure 30: Touch display with custom GUI.

the friction when a load is applied by the end effector to the self-locking mechanism. This mechanism requires little energy because the motor is only programmed to rotate without load.

Obstructing fast movements could however also induce hazardous situations. For example, on the brink of tipping over in the exoskeleton, the user could be tended to swiftly move the arm. An option could be to constrain only the upward motions, i.e. leaving the upper side of the slot open.

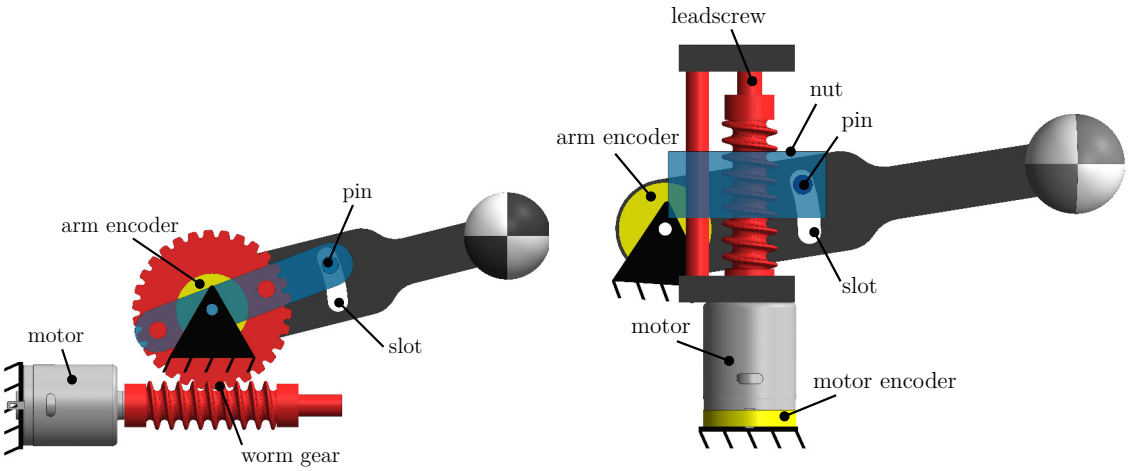

(a) (b)

Figure 31: Safety mechanism concepts for the arm support: dynamic end stop. (a) Rotary. (b) Linear.

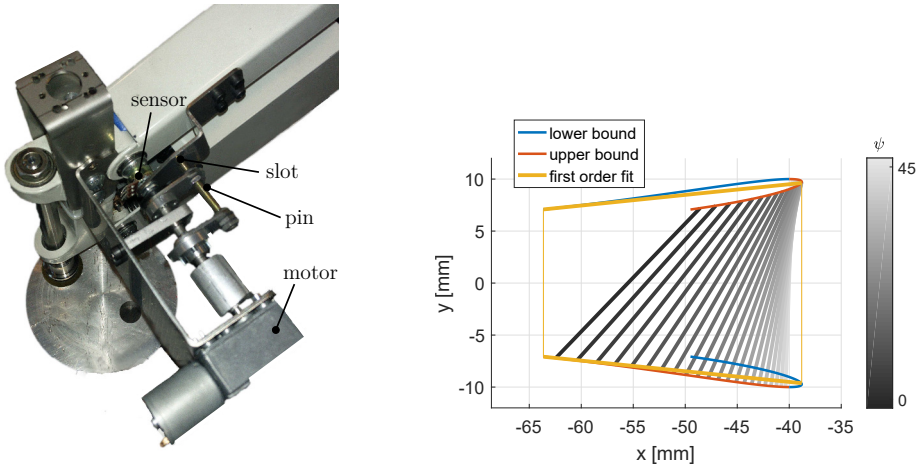

(a) (b)

Figure 32: (a) POC of the dynamic rotary end stop. (b) Determination of the shape of the slot for the linear dynamic end stop. The gradient gray lines indicate the pin motion with respect to the slot at a specific angle for positive ψ angles. Positive (in red) and negative bounds (in blue) bounds calculated for the slot. First order fit (yellow) of the slot shape for the safety mechanism.

4 DISCUSSION

This section discusses the results gained from this project. In this PDEng project several concepts for an industrial mobile lifting aid were devised and POCs were built. Unfortunately, due to time constrains it was not possible to thoroughly test and evaluate the WingMAS and AGB. Therefore it was also not possible to mount the AGB on the WingMAS (an impression of this implementation is shown in Figure 33a).

4.1 WINGMAS

The Wingmas exoskeleton is an unique exoskeleton for its high payload compensation and automatic compensation. Although the developed exoskeleton successfully sufficed the key requirement, it was still considered too impracticably for daily usage. There are several reasons why designing a successful heavy duty passive industrial exoskeleton is next to impossible.

First, when manipulating a payload with stretched arms the resulting moment would often be so large that the subject would tip over. Although the tipping point depends on the subjects body dimensions and stance, at straight stance a payload of a little as 12 kg could induce tipping over. A possible solution would be to limit the workspace to allow merely for manipulations close to the chest or to incorporate a counterweight.

Second, an exoskeleton will almost always impeded movements. Most notable impeded movement was walking. The added inertia of the exoskeleton is definitely noticeable and prolonged wearing was consired wearisome. It kown that it is difficult task to design an exoskeleton which lowers the metabolic rate. Only few researches have succesfully developed devices that lower metabolic rate [32, 36, 8].

Third, the acceptance of industrial exoskeletons among employees in general is low. An exoskeleton has to be close to perfection, little shortcoming could quickly be causing irritation by the wearer. Furthermore, the hassle of donning and doffing exoskeleton could result in disregardig the exoskeleton. Even with the agile Leavo, with proven ergnomical results [7], acceptance among employees is not a matter of course.

4.2 AGB

During the project the focus shifted from a full body exoskeleton to an automatically adjustable gravity balancer. The AGB is able to meet the expectations; it is able to adjust from 0 to 20 kg compensation within one second. Note, the desired 25 kg compensation

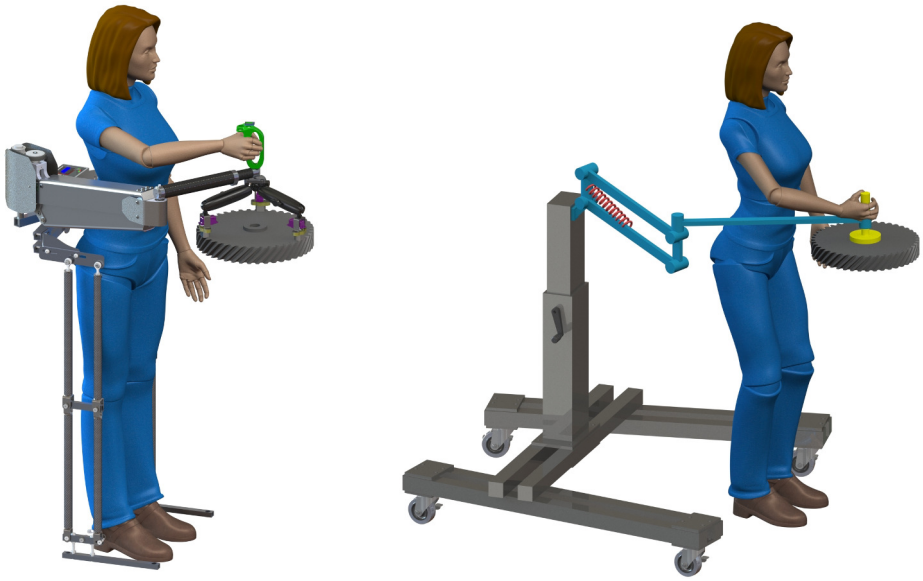

(a) (b)

Figure 33: CAD impression of the AGB, (a) integrated on the WingMAS (b) and integrated on a mobile cart.

was not obtained due to the safety limits and the AGB own weight. It should be noted that the performances was still constrained by software limits (motor angular velocity and battery maximum current).

Much effort has been put into the adjustment component. The desire was a large adjustment stroke (a) which resulted into a dissected shaft (see Figure 29b). Beyond the increased complexity, an adverse effect is decreased stiffness.

Multiple haptic control methods were evaluated. Measuring the payload with a force sensor offers a legion of application possibilities. However, it should be noted that proportional feedback could potential be hazardous; a positive feedback loop is obtained when the force sensor comes in contact with a rigid objects.

The AGB has the potential to be successfully deployed at the work floor. Currently, the bachelor student Nienke Bink is doing experiments with the AGB at Hankamp Gears. EMG measurements should quantify the effects of the lifting aid when performing a pick and place task. The design of the AGB could also be used for an updated and automated version the Seabo MAS; the MAS 2.

Keemink et al. studied the effects of an added damping for reaching motions [17]. The researchers found that adding position dependent damping forces could benefit manual manipulation of heavy objects. However, this would require actively controlled dampers which were deemed too complex to include to the AGB.

4.3 INTELLIGENT INDUSTRIAL MANIPULATORS

As mentioned, the project shifted from a full body exoskeleton to an arm support mounted on a (mobile) base. An impression of the opted solution, an AGB on a passive cart, is shown in Figure 35b. This solution takes advantage of the automatic compensation support of the AGB and of the mobility of a cart, while the operator movements remain unimpeded.

(a) (b) (c)

Figure 34: Intelligent industrial manipulators. (a) Stack@Ease (*Vanderlande*) (b) Ecopick [18] (c) Cobomanip (*Sarrazin-technologies*).

Few devices offer the same posiblititie, three intresting devices are shown in Figure 34. First, the Stack@Ease (*Vanderlande*) is a backage handling device for airport services. The payload is measured and the compensation is adjusted accordantly. It contains two springs, one to store energy for adjustment, similar to the mechanism discussed in Appendix E. In contrast to the AGB does the Stack@Ease not contain a leadscrew which greatly improves the efficiency of the secondary spring. Second, the Ecopick is a lift assistance device to aid workers in distribution centers [18]. It consists of an overhead boom and a cable. The boom is controlled by pressure sensors gloves. Third, the Cobomanip manipulator (*Sarrazin-technologies*) is capable of handing 100 kg [9]. The device features 4 DOF, each with an added motor to constrain specific movements.

4.4 CONCLUSION

This project explored possibilities for human augmentation devices for pick and place tasks at the work floor. The WingMAS exoskeleton successfully demonstrated the working principles for a passive industrial exoskeleton. The exoskeleton transfers the payload forces and moment to ground, alleviating the strain on the operator. The presented second version of the WingMAS features enhanced mobility and shorter donning and doffing times.

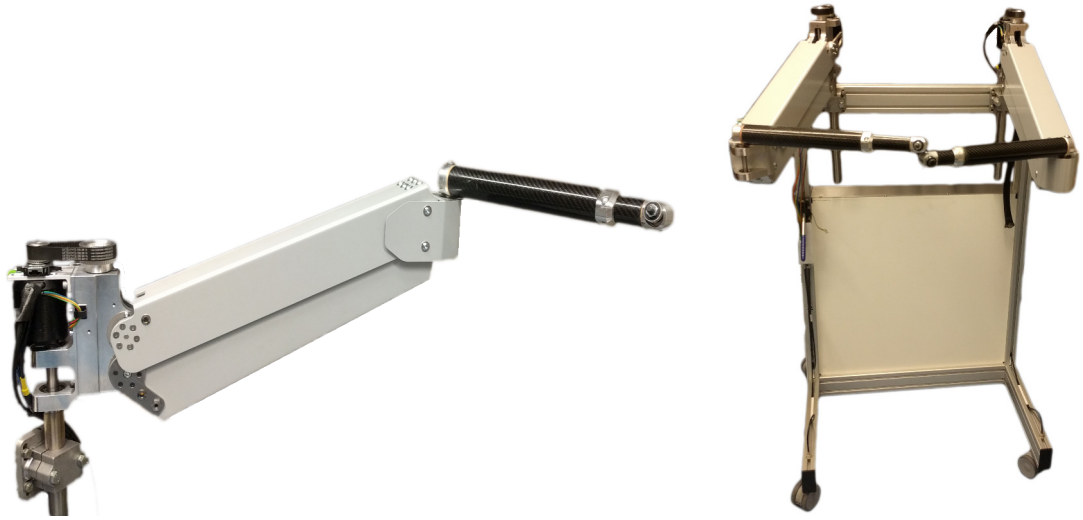

(a) (b)

Figure 35: (a) AGB. (b) Two AGBs on a cart, the experimental setup for patient carrying.

Nevertheless, a full body (semi-)passive exoskeleton was deemed not practical enough to be deployed at Hankamp Gears. Therefore the project shifted to a mobile base frame mounted gravity balancer. The AGB is an unique apparatus. Its capability to adjust the compensation from 0 to 20 kg within one second holds premise for various applications. Various haptic interfaces were evaluated to automatically adjust the compensation.

Deliverables were produced for experiments and Hankamp Gears and Siza; a single AGB on a base-frame and two AGBs on a cart respectively (see Figure 35).

BIBLIOGRAPHY

[1] Mohammad Abdoli-E and Joan M. Stevenson. The effect of on-body lift assistive device on the lumbar 3D dynamic moments and EMG during asymmetric freestyle lifting. *Clinical Biomechanics*, 23(3):372–380, 2008. ISSN 02680033. doi: 10.1016/j.clinbiomech.2007.10.012.

[2] Mohammad Abdoli-E, Michael J. Agnew, and Joan M. Stevenson. An on-body personal lift augmentation device (PLAD) reduces EMG amplitude of erector spinae during lifting tasks. *Clinical Biomechanics*, 21(5):456–465, 2006. ISSN 02680033. doi: 10.1016/j.clinbiomech.2005.12.021.

[3] Ruprecht Altenburger, Daniel Scherly, and Konrad S. Stadler. Design of a passive, iso-elastic upper limb exoskeleton for gravity compensation. *ROBOMECH Journal*, 3(1):12, 2016. ISSN 2197-4225. doi: 10.1186/s40648-016-0051-5. URL http://robomechjournal.springeropen.com/articles/10.1186/s40648-016-0051-5.

[4] Jose C. Barajas and Robert a. Paz. Autobalancing a generalized gravity equilibrator. *International Journal of Dynamics and Control*, (October 2014), 2015. ISSN 2195-268X. doi: 10.1007/s40435-015-0173-2. URL http://link.springer.com/10.1007/s40435-015-0173-2.

[5] Rogier Barents, Mark Schenk, Wouter D. van Dorsser, Boudewijn M. Wisse, and Just L. Herder. Spring-to-Spring Balancing as Energy-Free Adjustment Method in Gravity Equilibrators. *Journal of Mechanical Design*, 133(6):061010, 2011. ISSN 10500472. doi: 10.1115/1.4004101.

[6] T Bosch, S E Mathiassen, B Visser, M P de Looze, and J H van Dieën. The effect of work pace on workload, motor variability and fatigue during simulated light assembly work. *Ergonomics*, 54(2):154–168, 2011. ISSN 0014-0139. doi: 10.1080/00140139.2010.538723.

[7] Tim Bosch, Jennifer van Eck, Karlijn Knitel, and Michiel de Looze. The effects of a passive exoskeleton on muscle activity, discomfort and endurance time in forward bending work. *Applied Ergonomics*, 54:212–217, 2016. ISSN 18729126. doi: 10.1016/j.apergo.2015.12.003. URL http://dx.doi.org/10.1016/j.apergo.2015.12.003.

[8] Steven H. Collins, M. Bruce Wiggin, and Gregory S. Sawicki. Reducing the energy cost of human walking using an unpowered exoskeleton. *Nature*, 522(7555):212–215, 2015. ISSN 0028-0836. doi: 10.1038/nature14288. URL http://dx.doi.org/10.1038/nature14288.

[9] Olivier David, List Interactive, Gif Yvette, Sylvain André, Sarrazin Technologies, Perrecy Les Forges, Fares Kfoury, List Interactive, and Gif Yvette. Cobomanip : a new generation of Intelligent Assist Device Summary / Abstract Mechanical design Kinematic architecture. pages 93–100, 2014.

[10] Michiel P. de Looze, Tim Bosch, Frank Krause, Konrad S. Stadler, and Leonard W. O'Sullivan. Exoskeletons for industrial application and their potential effects on physical work load. *Ergonomics*, 0139(December):1–11, 2015. ISSN 0014-0139. doi: 10.1080/00140139.2015.1081988. URL http://www.tandfonline.com/doi/full/10.1080/00140139.2015.1081988.

[11] P.E. Dupont. Friction modeling in dynamic robot simulation. *Proceedings., IEEE International Conference on Robotics and Automation*, pages 1370–1376, 1990. doi: 10.1109/ROBOT.1990.126193.

[12] W.A. Gool. *Tillen tijdens werk*. 2012. ISBN 9789055499359.

[13] Sandra G. Hart and Lowell E. Staveland. Development of NASA-TLX (Task Load Index): Results of Empirical and Theoretical Research. *Advances in Psychology*, 52(C): 139–183, 1988. ISSN 01664115. doi: 10.1016/S0166-4115(08)62386-9.

[14] Just L Herder. Energy Free Systems, 2001.

[15] Koen Heuver. 2D Tilhulp: ontwerp van een 2 dimensionale robotarm. (053), 2014.

[16] Human Performance Research Group. NASA Task Load Index User Manual v. 1.0, 1986.

[17] Arvid Q L Keemink, Richard I K Fierkens, Joan Lobo-Prat, Jack S F Schorsch, David A. Abbink, Jeroen B J Smeets, and Arno H A Stienen. Using position dependent damping forces around reaching targets for transporting heavy objects: A Fitts law approach. *Proceedings of the IEEE RAS and EMBS International Conference on Biomedical Robotics and Biomechatronics*, 2016-July:1323–1329, 2016. ISSN 21551774. doi: 10.1109/BIOROB.2016.7523815.

[18] Steven A. Lavender, Pei Ling Ko, and Carolyn M. Sommerich. Biomechanical evaluation of the Eco-Pick lift assist: A device designed to facilitate product selection tasks in distribution centers. *Applied Ergonomics*, 44(2):230–236, 2013. ISSN 00036870. doi: 10.1016/j.apergo.2012.07.006. URL http://dx.doi.org/10.1016/j.apergo.2012.07.006.

[19] Heedon Lee, Wansoo Kim, Jungsoo Han, and Changsoo Han. The technical trend of the exoskeleton robot system for human power assistance. *International Journal of Precision Engineering and Manufacturing*, 13(8):1491–1497, 2012. ISSN 12298557. doi: 10.1007/s12541-012-0197-x.

[20] Ralph Macke. Investigation into lumbar force and back torque compensation in body-mounted lifting aids. 2015.

[21] Jawad Masood, Jesus Ortiz, Jorge Fernandez, Luis A. Mateos, and Darwin G. Caldwell. Mechanical design and analysis of light weight hip joint Parallel Elastic Actuator for industrial exoskeleton. *Proceedings of the IEEE RAS and EMBS International Conference on Biomedical Robotics and Biomechatronics*, 2016-July(August):631–636, 2016. ISSN 21551774. doi: 10.1109/BIOROB.2016.7523696.

[22] M a Nussbaum, D B Chaffin, and G Baker. Biomechanical analysis of materials handling manipulators in short distance transfers of moderate mass objects: joint strength, spine forces and muscular antagonism. *Ergonomics*, 42(12):1597–618, 1999. ISSN 0014-0139. doi: 10.1080/001401399184703. URL http://www.ncbi.nlm.nih.gov/pubmed/10643403.

[23] Cal Osha, Consultation Service, and Education Unit. Ergonomic guidelines for manual material handling. *DHHS (NIOSH) Publication*, page 131, 2007. ISSN 1098-6596. doi: 10.1017/CBO9781107415324.004. URL http://www.cdc.gov/niosh/docs/2007-131/pdfs/2007-131.pdf.

[24] Maarten Pijper. Work space analysis in order to obtain data for the desin of a haptic lifting aid. 2013.

[25] Tariq Rahman, Whitney Sample, Shanmuga Jayakumar, Marilyn Marnie King, Jin Yong Wee, Rahamim Seliktar, Michael Alexander, Mena Scavina, and Alisa Clark. Passive exoskeletons for assisting limb movement. *Journal of rehabilitation research and development*, 43(5):583–590, 2006. ISSN 0748-7711. doi: 10.1682/JRRD.2005.04.0070.

[26] Alexander Rosendaal. Design of a user-friendly safe gravity compensation device to assist with lifting during pick and place tasks. 2015.

[27] Louise Schneider. Ontwerp en realisatie van een regelsysteem voor de bewegende arm van een exoskelet. 2016.

[28] J F Schorsch and D A Abbink. Lifting Tasks for Different Levels of Weight Compensation. pages 426–431, 2014.

[29] M G Schuurman. Developing a Haptic ' Slave Hand ' for Grabbing and Lifting Objects Intuitively for Industrial Purposes . 2015.

[30] Arno H A Stienen. Development of novel devices for upper-extremity rehabilation. 2009.

[31] Brent L. Ulrey and Fadi A. Fathallah. Effect of a personal weight transfer device on muscle activities and joint flexions in the stooped posture. *Journal of Electromyography*

and Kinesiology, 23(1):195–205, 2013. ISSN 10506411. doi: 10.1016/j.jelekin.2012.08.014. URL http://dx.doi.org/10.1016/j.jelekin.2012.08.014.

[32] Wietse Van Dijk. Human Exoskeleton Interaction. 1, 2015. ISSN 1098-6596. doi: 10.1017/CBO9781107415324.004. URL http://resolver.tudelft.nl/uuid:8cf37c65-a48c-476e-8dcc-eb97c06c26d9{#}.VtBSjgH3jKw.mendeley.

[33] Wouter D. van Dorsser, Rogier Barents, Boudewijn M. Wisse, and Just L. Herder. Gravity-Balanced Arm Support With Energy-Free Adjustment. *Journal of Medical Devices*, 1(2):151, 2007. ISSN 19326181. doi: 10.1115/1.2736400.

[34] M.A van Hirtum. SEP: 2 DOF diagnostic elbow stretch perturbator. 2014.

[35] E V Velu. Development of an exoskeleton for the lower extremities as passive load Confidential. 2016.

[36] Conor James Walsh, Ken Endo, and Hugh Herr. A Quasi-Passive Leg Exoskeleton for Load-Carrying Augmentation. *International Journal of Humanoid Robotics*, 04(3): 487–506, 2007. ISSN 0219-8436. doi: 10.1142/S0219843607001126.

[37] Thomas Waters, Vern Putz-Anderson, and Arun Garg. Quick Guide for the NIOSH lifting equation, 1994.

[38] Michael Wehner, David Rempel, and Homayoon Kazerooni. Lower Extremity Exoskeleton Reduces Back Forces in Lifting. *ASME 2009 Dynamic Systems and Control Conference, Volume 2*, (OCTOBER 2009):49–56, 2009. doi: 10.1115/DSCC2009-2644. URL http://link.aip.org/link/ASMECP/v2009/i48937/p49/s1{&}Agg=doi.

[39] Brett H. Whitfield, Patrick A. Costigan, Joan M. Stevenson, and Catherine L. Smallman. Effect of an on-body ergonomic aid on oxygen consumption during a repetitive lifting task. *International Journal of Industrial Ergonomics*, 44(1):39–44, 2014. ISSN 01698141. doi: 10.1016/j.ergon.2013.10.002.

[40] Boudewijn M. Wisse, Wouter D. Van Dorsser, Rogier Barents, and Just L. Herder. Energy-free adjustment of gravity equilibrators using the virtual spring concept. *2007 IEEE 10th International Conference on Rehabilitation Robotics, ICORR'07*, 00(c):742–750, 2007. doi: 10.1109/ICORR.2007.4428508.

[41] Fiona Wixted and Leonard O Sullivan. the Effect of Automated Manufacturing Environments on Employee Health. (ESENER 2012):80–91, 2013.

[42] Keijiro Yamamoto, Mineo Ishii, Kazuhito HYODO, Toshihiro Yoshimitsu, and Takashi Matsuo. Development of Power Assisting Suit (Miniaturization of Supply System to Realize Wearable Suit). *JSME International Journal Series C*, 46(3):923–930, 2003. ISSN 1344-7653. doi: 10.1299/jsmec.46.923. URL http://joi.jlc.jst.go.jp/JST.JSTAGE/jsmec/46.923?from=CrossRef.

Appendix

A

INDUSTRIAL EXOSKELETONS

A.1 HEAVY DUTY EXOSKELETONS

(a) (b) (c) (d) (e)

Figure 36: (a) RB3D Hercule v3. (b) DMSE (c) Hyundai. (d) Kawasaki Power Assist Suit. (e) Cyberdyne HAL 5.

A.2 ARM SUPPORT EXOSKELETONS

(a) (b) (c) (d)

Figure 37: (a) Exhauss. (b) Levitate. (c) Skel-ex (d) Robo-mate.

(a) (b) (c)

(d) (e) (f)

Figure 38: (a) Activelink. (b) Cyberdyne HAL labor support. (c) Hyundai. (d) Innophys muscle suit. (e) Laevo. (f) Robomate.

B FREE BODY DIAGRAMS

B.1 FREE BODY DIAGRAM ARM SUPPORT

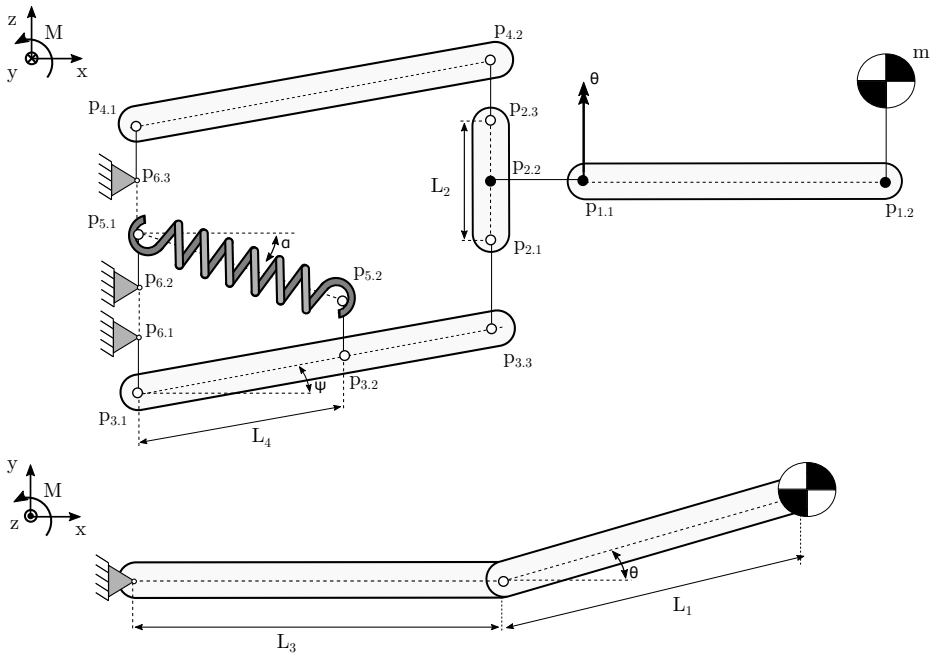

	F_x	F_y	F_z	M_x	M_y	M_z
$p_{1.1}$	0	0	$-F_{1.2,z}$	$\sin(\theta)\, L\, F_{1.2,z}$	$\cos(\theta)\, L\, F_{1.2,z}$	0
$p_{1.2}$	0	0	m g	0	0	0
$p_{2.1}$	$\frac{M_{2.2,y}}{L_2}$	$\frac{M_{2.2,x}}{L_2}$	$F_{2.2,z} + \tan(\psi)\, F_{2.1,x}$	0	0	0
$p_{2.2}$	0	0	$-F_{1.1,z}$	$-M_{1.1,x}$	$-M_{1.1,y}$	0
$p_{2.3}$	$\frac{M_{2.2,y}}{L_2}$	$\frac{M_{2.2,x}}{L_2}$	$\tan(\psi)\, F_{2.3,x}$	0	0	0
$p_{3.1}$	$-F_{3.3,x} - F_{3.2.x}$	$-F_{3.3,y} - F_{3.2.y}$	$-F_{3.3,z} - F_{3.2.z}$	0	0	$F_{3.3,y}\, L_3$
$p_{3.2}$	$-F_{5.2,x}$	0	$-F_{5.2,z}$	0	0	0
$p_{3.3}$	$-F_{2.1,x}$	$-F_{2.1,x}$	$-F_{2.1,x}$	0	0	0
$p_{4.1}$	$-F_{4.2,x}$	$-F_{4.2,y}$	$-F_{4.2,z}$	0	0	$F_{4.2,y}\, L_3$
$p_{4.2}$	$-F_{2.3,x}$	$-F_{2.3,y}$	$-F_{2.3,z}$	0	0	0
$p_{5.1}$	$\cos(\alpha)\, F_{sp}$	0	$\sin(\alpha)\, F_{sp}$	0	0	0
$p_{5.2}$	$-F_{5.1,x}$	0	$-F_{5.1,z}$	0	0	0

Figure 39: Free body diagram arm support.

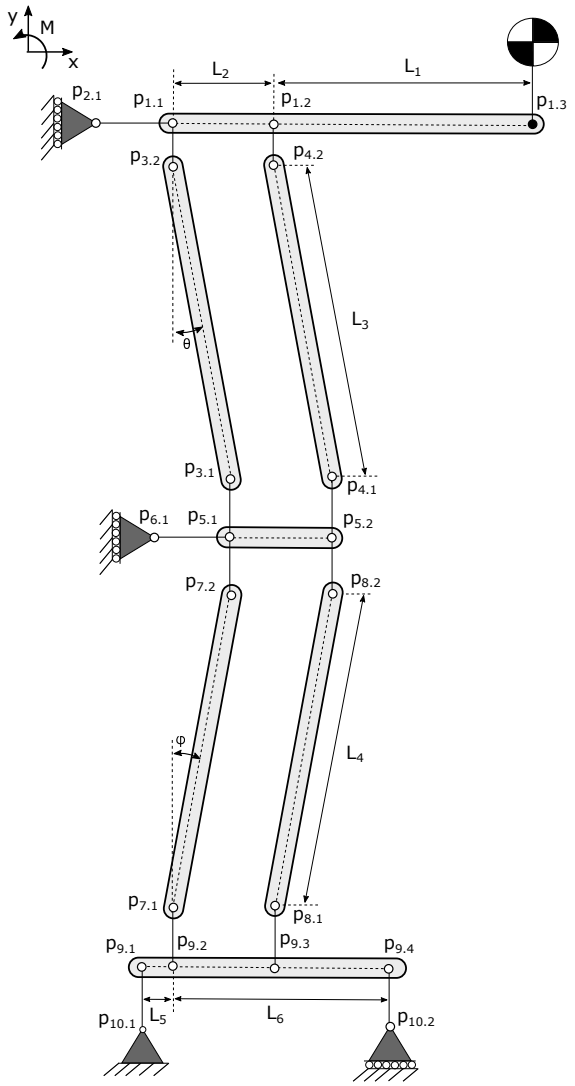

	F_x	F_z
$p_{1.1}$	$\tan(\theta)F_{1.1,z}$	$-F_{1.3,z}\left(\frac{L_1}{L_2}+1\right)$
$p_{1.2}$	$\tan(\theta)F_{4.2,z}$	$\frac{L_1}{L_2}F_{1.3,z}$
$p_{1.3}$	0	$-m\,g$
$p_{2.1}$	$-F_{1.1,x}$-$F_{1.2,x}$	0
$p_{3.1}$	$-F_{3.2,x}$	$-F_{3.2,z}$
$p_{3.2}$	$-F_{1.1,x}$	$-F_{1.1,z}$
$p_{4.1}$	$-F_{4.2,x}$	$-F_{4.2,z}$
$p_{4.2}$	$-F_{1.2,x}$	$-F_{1.2,z}$
$p_{5.1}$	$-F_{3.1,x}-F_{7.2.x}$	$-F_{3.1,z}$
$p_{5.2}$	$-F_{4.1,x}-F_{8.2.x}$	$-F_{4.1,z}$
$p_{6.1}$	$-F_{5.1,x}$-$F_{5.2,x}$	0
$p_{7.1}$	$-F_{7.2,x}$	$-F_{7.2,z}$
$p_{7.2}$	$\tan(\phi)F_{5.1,z}$	$-F_{5.1,z}$
$p_{8.1}$	$-F_{8.2,x}$	$-F_{8.2,z}$
$p_{8.2}$	$\tan(\phi)F_{5.2,z}$	$-F_{5.2,z}$
$p_{9.1}$	$-F_{9.2,x}$-$F_{9.3,x}$	$-F_{9.2,z}-F_{9.3,z}-F_{9.4,z}$
$p_{9.2}$	$-F_{7.1,x}$	$-F_{7.1,z}$
$p_{9.3}$	$-F_{8.1,x}$	$-F_{8.1,z}$
$p_{9.4}$	0	$\frac{-L_5\,F_{9.2,z}-(L_5+L_2)F_{9.3,z}}{L_5+L_6}$
$p_{10.1}$	$-F_{9.1,x}$	$-F_{9.1,z}$
$p_{10.2}$	0	$-F_{9.4,z}$

Figure 40: Free body diagram leg support: double parallelogram.

C

GAS SPRING

Gas springs typically contain a high pretension and are therefore suitable to be used in a gravity balancer without a cable, while still exhibiting ideal spring behaviour. The force of the gas spring (F_{sp}) is described by the equation:

$$F_{sp} = F_0 + P\,F_0 \frac{L_s}{L_m} \tag{11}$$

Where L_s is the current gas spring stroke, L_m the gas spring maximum stroke and F_0 the initial spring force. The spring stiffness is determined by:

$$k = \frac{P\,F_0}{L_m} \tag{12}$$

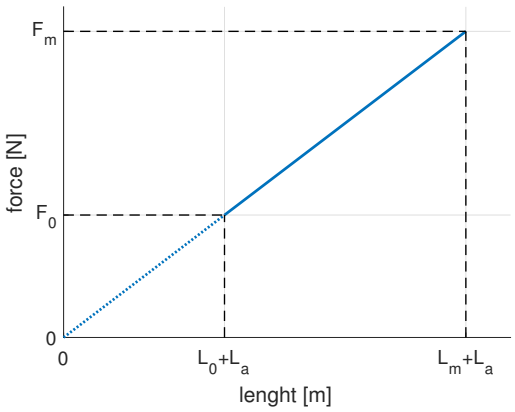

Figure 41: By adding a length L_a an ideal gas spring could be created.

Ideal spring behaviour could be enforced by adding a length (L_a) to L_0 as shown in Figure 41.

$$F_0 = (L_0 + L_a)\,k \tag{13}$$

Rewritten to L_a and substitution of k.

$$L_a = \frac{F_0 - L_0\,k}{k} \tag{14}$$

Spring balancer equation:

$$a\,k\,r = m\,g\,L \tag{15}$$

By combining Equation 12 and Equation 15 we get:

$$k = \frac{P\,F_0}{L_m} = \frac{a\,r}{m\,g\,L} \tag{16}$$

The gas spring has to fit in the gravity balancer, therefore constrains for the minimum (s_{min}) and maximum (s_{max}) spring length are applied.

$$L_0 \quad < s < \quad L_0 + L_m$$

The spring length (s) can be found with:

$$s = \sqrt{a^2 + r^2 - 2\,a\,r\,\sin(\phi)} \tag{17}$$

The leadscrew attachment position (a) is contained between 0.03 and 0.1 m and $r = L$. The P, F_0 and L_m are design parameters. This leads to a solution matrix shown in Figure 42

Both positive and negative L_a are theoretically possible. However, a negative L_a results in a protruded gas spring. The plot shows that a progression of $P \approx 0.25$ provides most suitable solutions for L_a.

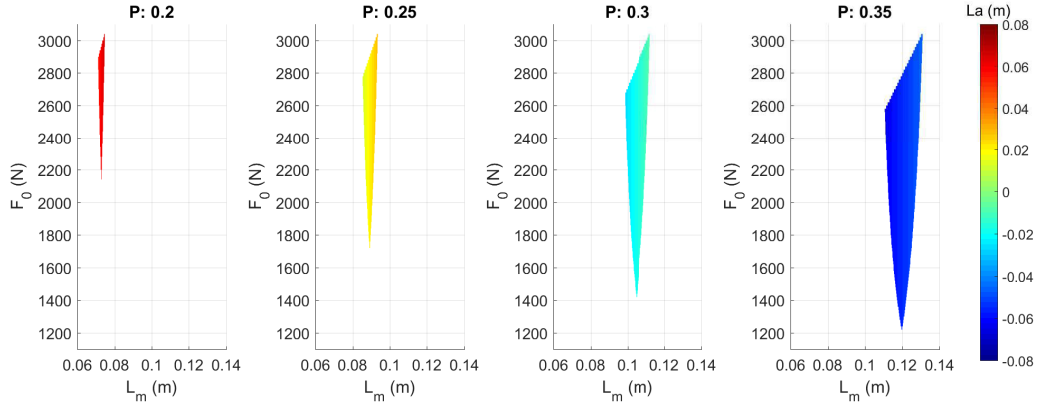

(a)

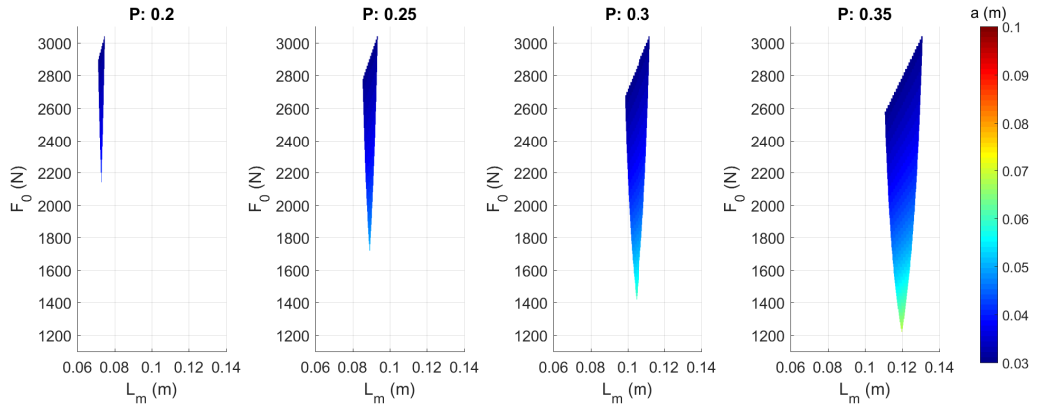

(b)

Figure 42: Gas spring parameter solution grid with different max strokes and initial force. (a) Additional length (L_a). (b) Spring leadscrew attachment (a).

D

COMPONENTS WITH THEIR KEY FEATURES

D.1 POC ADJUSTMENT MECHANISM V1

DC Motor

148867, Maxon

rated voltage	24 V
rated Power	150 W
torque constant	0.3 Nm/A
winding resistance	0.299 Ω
weight	0.48 kg

Motor endocer

225787, Maxon

counts per turn	1024
operating voltage	5 V
number of channels	3

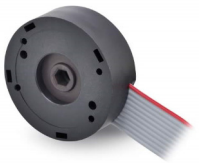

H-Bridge

18v25, Pololu

voltage	5.5-30 V (6S)
continuous current	25 A
current sense	

Micro controller

Arduino Mega

clock speed	16 MHz
data memory	8 KB
operation voltage	5 V
analogue input ports	16

Load bar

CZL635, UCHI

range	0 - 5 kg
rated output	1.09 ∓ 0.5
non-linearity	± 0.005 % FS
hysteresis	± 0.005 % FS
repeatability	± 0.005 % FS

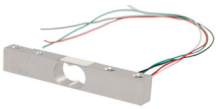

Amplifier

SG-3016, ICP-DAS

voltage range	0..5,0..10,+/-5,+-10 V
strain gauge input	+/-10, +/-20, +/-30, +/-50, +/-100 mV

Battery

Nano-tech 2650mah 6S, Turnigy

voltage	5.5-30 V (6S)
continuous current	25 A
current sense	

D.2 POC ADJUSTMENT MECHANISM V2

Outrunner motor

SII 4035 250KV, Scorpion

rated voltage	44 V
continuous power	2700 W
torque constant	0.03 Nm/A
winding resistance	0.037 Ω
weight	0.45 kg

Brushless controller

hobbyking X-Car 120A, Hobbyking

voltage	7.4-11.V (2-3S)
continuous current	120 A
peak current	480 A
sensorless/hall sensors	
5V BEC	

Microcontroller

Arduino Mega

clock speed	16 MHz
data memory	8 KB
operation voltage	5 V
analogue input ports	16

Accelerometer

MPU 6050, Invernsense

breakout board	GY-521
DOF	6
accelerometer	± 2,± 4,± 8, ± 16 g
gyro	± 250,± 500,± 1000, ± 2000 deg/s

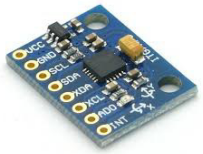

Load bar

CZL635, UCHI

range	0 - 5 kg
rated output	1.09 ∓ 0.5
non-linearity	± 0.005 % FS
hysteresis	± 0.005 % FS
repeatability	± 0.005 % FS

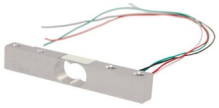

Amplifier

SG-3016, ICP-DAS

voltage range	0..5,0..10,+/-5,+-10 V
strain gauge input	+/-10, +/-20, +/-30, +/-50, +/-100 mV

Battery

Nano-tech 2650mah 6S, Turnigy

voltage	5.5-30 V (6S)
continuous current	25 A
current sense	

D.3 AGB

Outrunner motor

Motor 6374, DIY Electric Skateboard

rated voltage	44 V
continuous power	3200 W
torque constant	0.042 Nm/A
winding resistance	0.05 Ω
weight	0.8 kg
integrated hall sensors	

Brushless controller

VESC v4.12

clock speed	120 MHz
data memory	32 MB SDRAM
operating voltage	3.3 V
analogue input ports	6

Microcontroler

LPC 4088, Embedded artist

clock speed	120 MHz
data memory	32 MB SDRAM
operating voltage	3.3 V
analogue input ports	6

Battery with BMS

12S3P Samsung 25R , Energus Power Solutions

chemistry	INR (NCA)
configuration	12s3p
capacity	324 Wh
nominal voltage	43.2 V
max continuous current	60 A %
max peak current	300 A
weight	1.62 kg

DC motor

25Dx48L , Pololu

rated voltage	12 V
encoder counts	48
stall torque	0.17 Nm
no load speed	235.6 rad/s

H-Bridge

VNH5019, Pololu

operating voltage	5.5 - 24 V
continuous current	12 A
Peak current	30 A
current sense	

Load cell

TAS 606, HTC Sensor

range	0 - 50 kg
rated output	1.5 ∓ 0.5
non-linearity	± 0.3 % FS
hysteresis	± 0.3 % FS
repeatability	± 0.3 % FS

Amplifier

SG-3016, ICP-DAS

voltage range	0..5,0..10,+/-5,+-10 V
strain gauge input	+/-10, +/-20, +/-30, +/-50, +/-100 mV

Encoder

AS 5048, Broadcom

resolution	14 bit (16384)
interface	SPI
output	PWM
operating voltage	3.3 or 5 V

Battery monitor

BW-LY5 V1.2E, BaiWay Electronic

input voltage	12-48 V

TFT Touch screen

Nextion

screen size	3.5″
resolution	480x320

Step down converter

DC-DC HRD Converter

input voltage	24-48 V
output voltage	12 V
rated current	3 A
efficiency	80 %

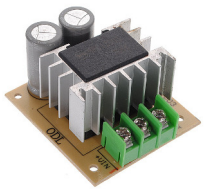

Linear potentiometer

PTB0144-2010BPA103, Bourns

range	100 mm
resistance	10 kΩ

Encoder

HEDM 5540, Broadcom

Range	± 1112 N
Non-linearity	0.5 %
Hysteresis	0.5 %
Non repeatability	0.1 %

Emergency button

84-5030.0020, EAO

D.4 Tripod magnet gripper

Stepper motor

BM2 705MG, Bluebird

rated voltage	6 V
torque	0.74 Nm
no load speed	0.17 rad/s
weight	0.031 kg

Magnet

Magjig 95, Magswitch

max load	105 kg
weight	0.2 kg

OLED screen

SSD1306, Adafruit

screen size	13″
resolution	128 x 54
monochrome oled	

Mount

RAM-B-201U-C Long, RAM Mounts

length	0.15 m

E

FAST ADAPTION WITH SECUNDARY SPRING

E.1 SECONDARY SPRING

Fast adaptations in compensation of the gravity balancer can be realised with a secondary spring in which energy is stored [5]. This appendix describes two concepts with a secondary spring.

E.1.1 *Theoretical concepts*

The secondary spring could be positioned in-line or trough a rotary link [14]. The two spring configuration are shown in Figure 43.

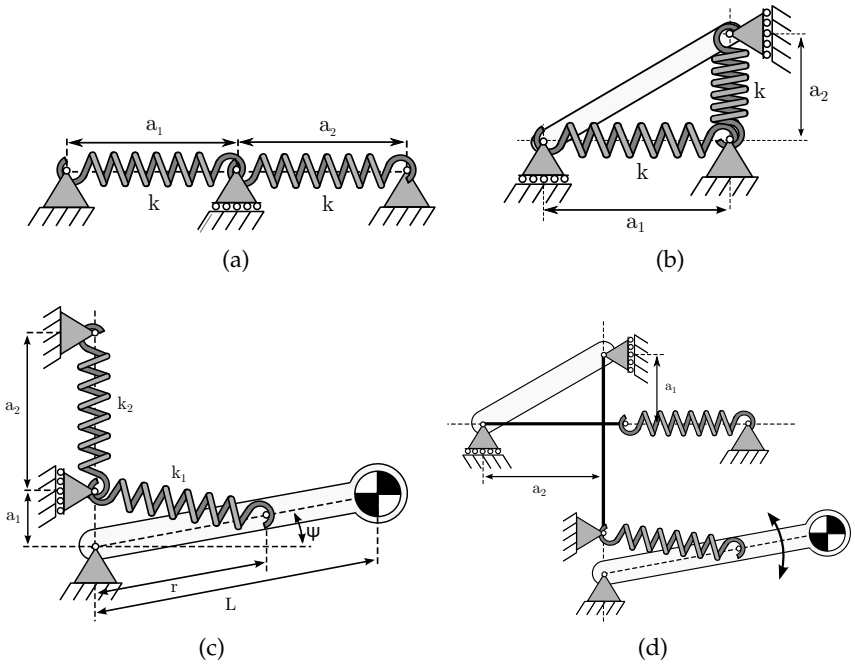

Figure 43: (a) Springs are in an in-line configuration. The system has a position where energy in minimum, the stiffness is $2 \cdot k$. (b) Rotary link configuration, the position of a does not change the total energy in the system. (c) Adjustment mechanism with in-line spring configuration (d) Adjustment mechanism with rotating link spring configuration.

The scenario of a gear grinder operator that picks up a gear from a low standing box and places it into the gear grinder is used for evaluation. The steps for adjustment of the gravity balancer this pick and place task are:

Table 3: Steps for adjustment when lifting an object.

Step 1.	Begin situation.
Step 2.	Fix angle and attach payload. Adjust spring tension to load with energy from secondary spring.
Step 3.	Raise the payload.
Step 4.	Fix angle and unload. Adjust spring tension to payload.
Step 5.	Move down and load secondary spring, return to 1.

The adjustment sequence according the the described steps for both mechanisms are shown in Figure 44.

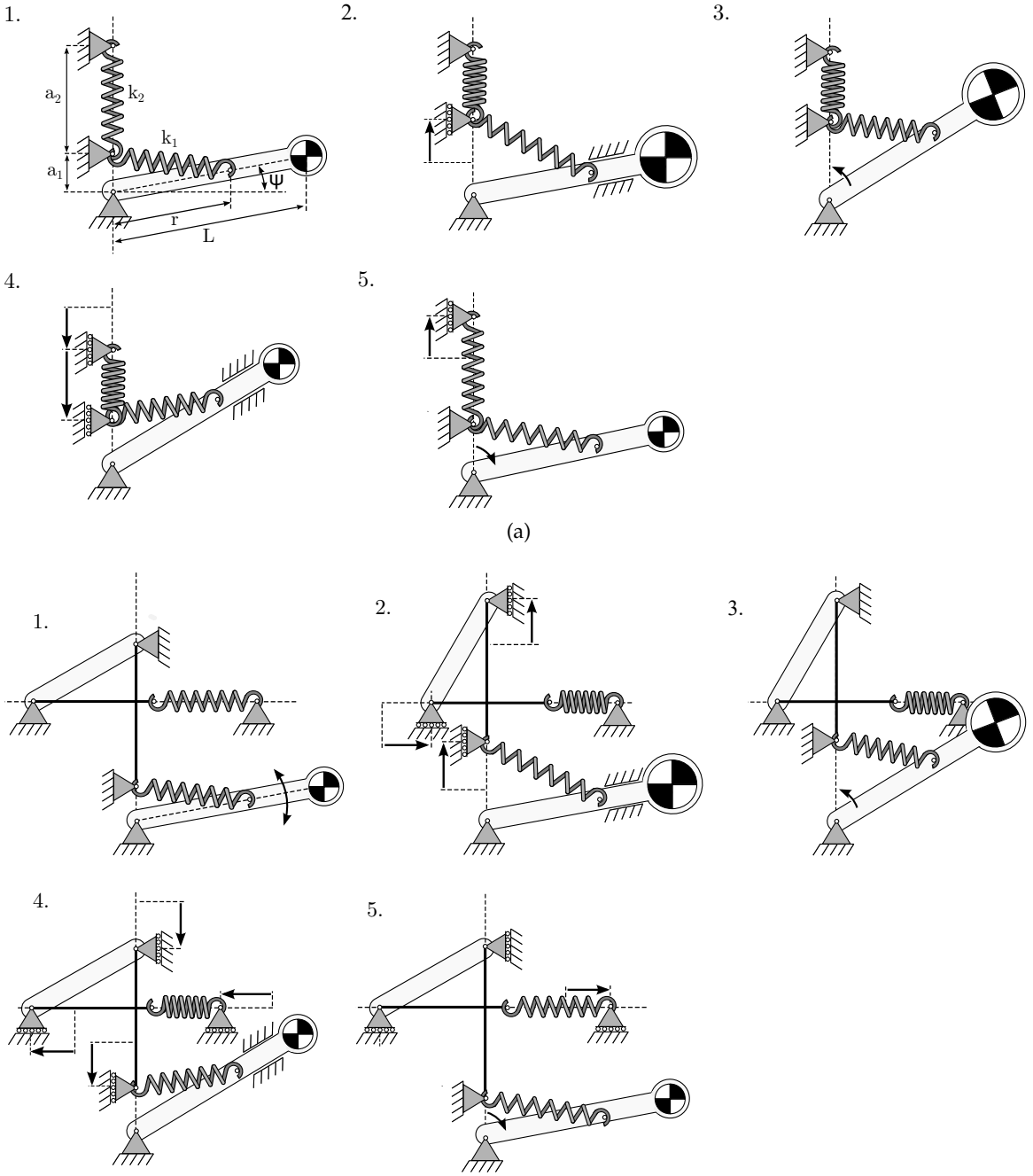

Figure 44: Gravity balancers with a secondary spring and linkage system for energy free adjustment.

F

AUTOMATIC ADJUSTMENT SIMULATION

A simulation was made in Matlab Simulink to verify the desired performance. Numerous commercial available components had been compared. This appendix describes the simulation model and presents an exemplary simulation result.

F.1 SIMULATION MODEL

The control schemes used for the simulation are presented Figure 45. The associated parameters are given in Table 4.

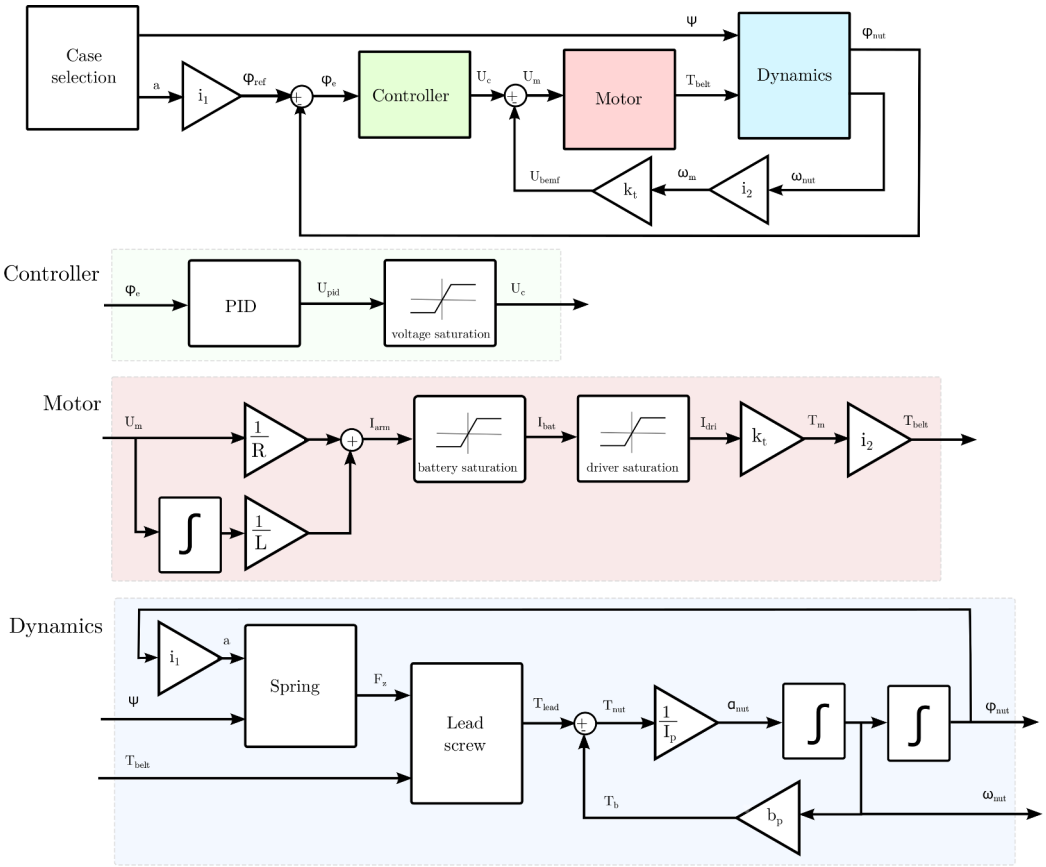

Figure 45: Control diagrams of the AGB dynamics simulation. (a) Top level. (b) Controller. (c) Motor. (d) Dynamics.

Table 4: Simulation parameters.

VARIABLE	VALUE	UNITS	DESCRIPTION
i_1	$4.78 \cdot 10^{-4}$	m	gear ratio lead screw
a	[0.006,0.08,0.08,0.08,0.006,0.006]	m	reference spring attachment height
ψ	[-60,-60,60,-60,60]	rad	gravity balancer angle
m	[1,25,25,25,1,1]	kg	payload
l	0.003	m	leadscrew pitch
d	0.012	m	leadscrew diameter
μ_l	0.12	-	leadscrew friction coefficient
μ_b	0.0020	-	bearing friction coefficient
P	1	-	proportional gain controller
I	0	-	integral gain controller
D	0	-	differential gain controller
I_{bat}	60	A	max battery current
U_{bat}	48	V	max battery voltage
I_{dri}	100	A	max driver current
U_{dri}	60	V	max driver voltage
mot_{kt}	0.038	Nm/A	torque constant
mot_L	0.018	H	motor inductance
ϕ_{ref}		rad	reference lead screw angle
ϕ_{nut}		rad	nut angle
ϕ_e		rad	error angle
ω_{nut}		rad/s	nut angular velocity
ω_m		rad/s	motor angular velocity
α_m		rad/s^2	motor angular acceleration
U_m		V	motor voltage
U_c		V	controller output
U_{bemf}		V	back EMF
I_{arm}		A	current motor armature
T_m		Nm	torque motor
T_{belt}		Nm	torque motor after belt
T_{lead}		Nm	torque leadscrew
T_{nut}		Nm	torque lead screw nut
T_b		Nm	torque damping lead screw

The block *spring* computes the vertical force (F_z) on the adjustment point a with:

$$F_z = -a\,k + r\,k\,\sin(\psi) \tag{18}$$

The block *leadscrew* computes the required torque to raise (T_{raise}) and to lower (T_{lower}) the leadscrew nut with a negative force (F_z) is give by:

$$T_{raise} = \frac{F_z\,d}{2}\left(\frac{l + \pi\,\mu_l\,d\,\sec(\alpha)}{\pi\,d - \mu_l\,l\,\sec(\alpha)}\right) \tag{19}$$

$$T_{lower} = \frac{F_z\,d}{2}\left(\frac{\pi\,\mu_l\,d\,\sec(\alpha) - l}{\pi\,d + \mu_l\,l\,\sec(\alpha)}\right) \tag{20}$$

Where d is the leadscrew diameter, l the leadscrew pitch and α the leadscrew angle. The friction (μ_l) is estimated to be 0.12 (based on a greased bronze nut and steel leadscrew).

Kinetic friction is not implemented [11]. The motor is connected with timing belt, the torque (T_{belt}) drives the leadscrew. The leadscrew friction is implemented as:

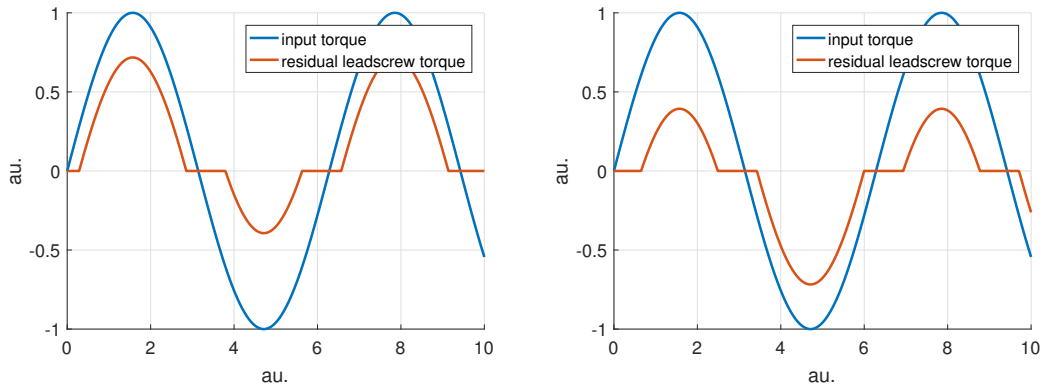

Figure 46: Residual torque on leadscrew when a motor torque (sinusoidal) and vertical force are applied on the leadscrew. (a) positive vertical force. (b) negative vertical force.

$$T_{lead} = \left\{ \begin{array}{ll} 0, & \text{for } T_{lower} < T_{belt} < T_{raise} \\ T_{belt} - T_{raise}, & \text{for } T_{belt} > T_{raise} \\ T_{belt} - T_{lower}, & \text{for } T_{belt} < T_{lower} \end{array} \right\} \tag{21}$$

The implemented leadscrew friction model is clarified in Figure 46. Subsequently, the torque resulting from bearing friction $T_{bearing}$ is addressed:

$$T_{bearing} = 0.5\,\mu_b\,F_z\,d \tag{22}$$

The bearing friction, μ_b, is determined at 0.0020[1]. The friction is implemented in a similar fashion as the leadscrew friction:

$$T_{nut} = \left\{ \begin{array}{ll} 0, & \text{for } T_{nut} < T_{bearing} \\ T_{nut} - T_{bearing}, & \text{for } T_{nut} > T_{bearing} \end{array} \right\} \tag{23}$$

F.2 SIMULATION RESULTS

The simulations provided valuable insights in the performance of the AGB. Numerous motors with different gear ratios were tested. The results for the final setup are presented in Figure 47. The selected components could be found in Appendix D.

1 SKF deep groove ball bearings

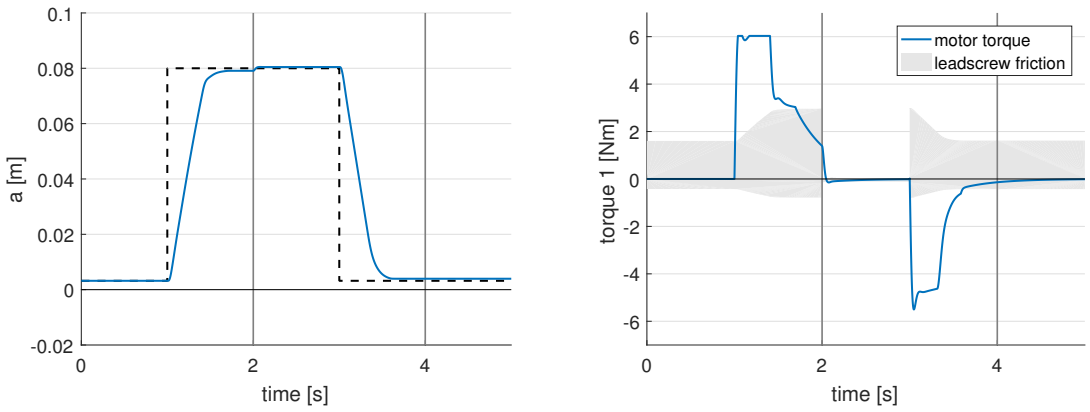

(a) (b)

Figure 47: AGB drivetrain simulation results. After one second the compensation is set from 0 to 25 kg and after three seconds the compensation is set to 0 kg again.

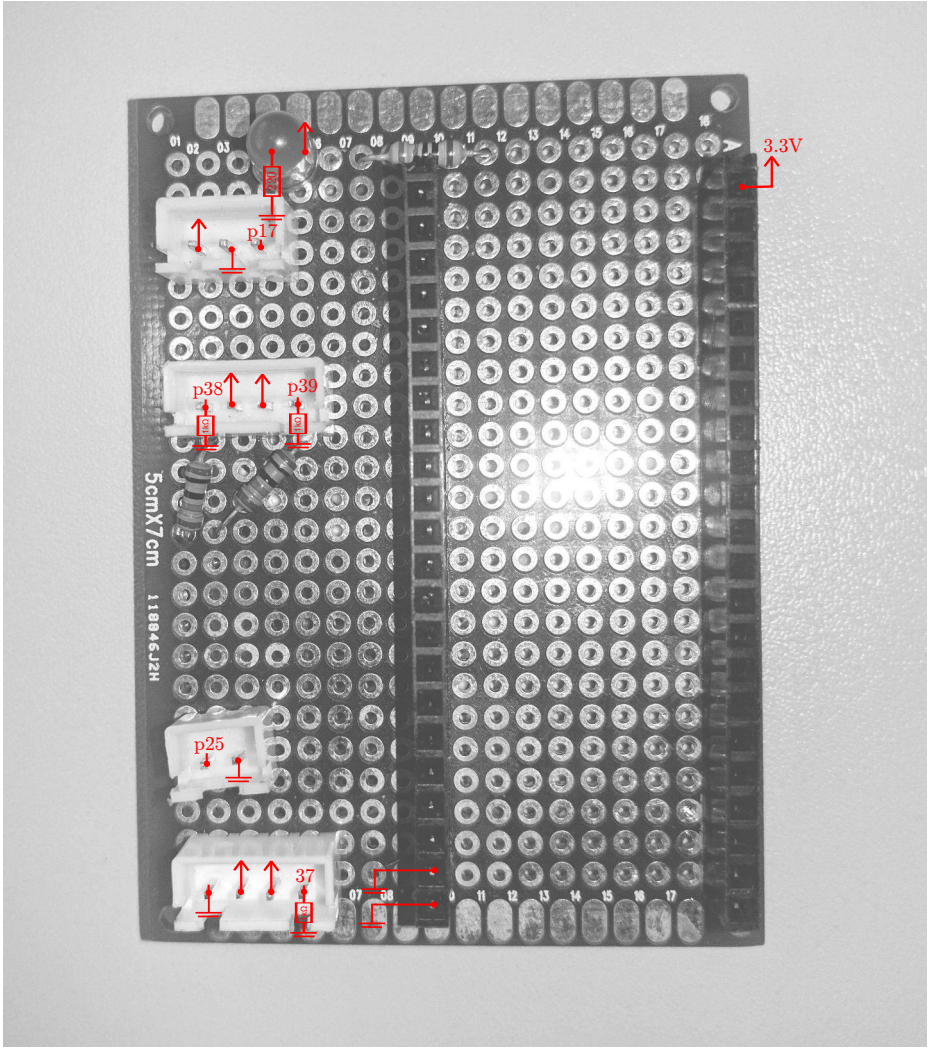

Figure 48: Custom made MBED EA LPC4088 shield pinout.

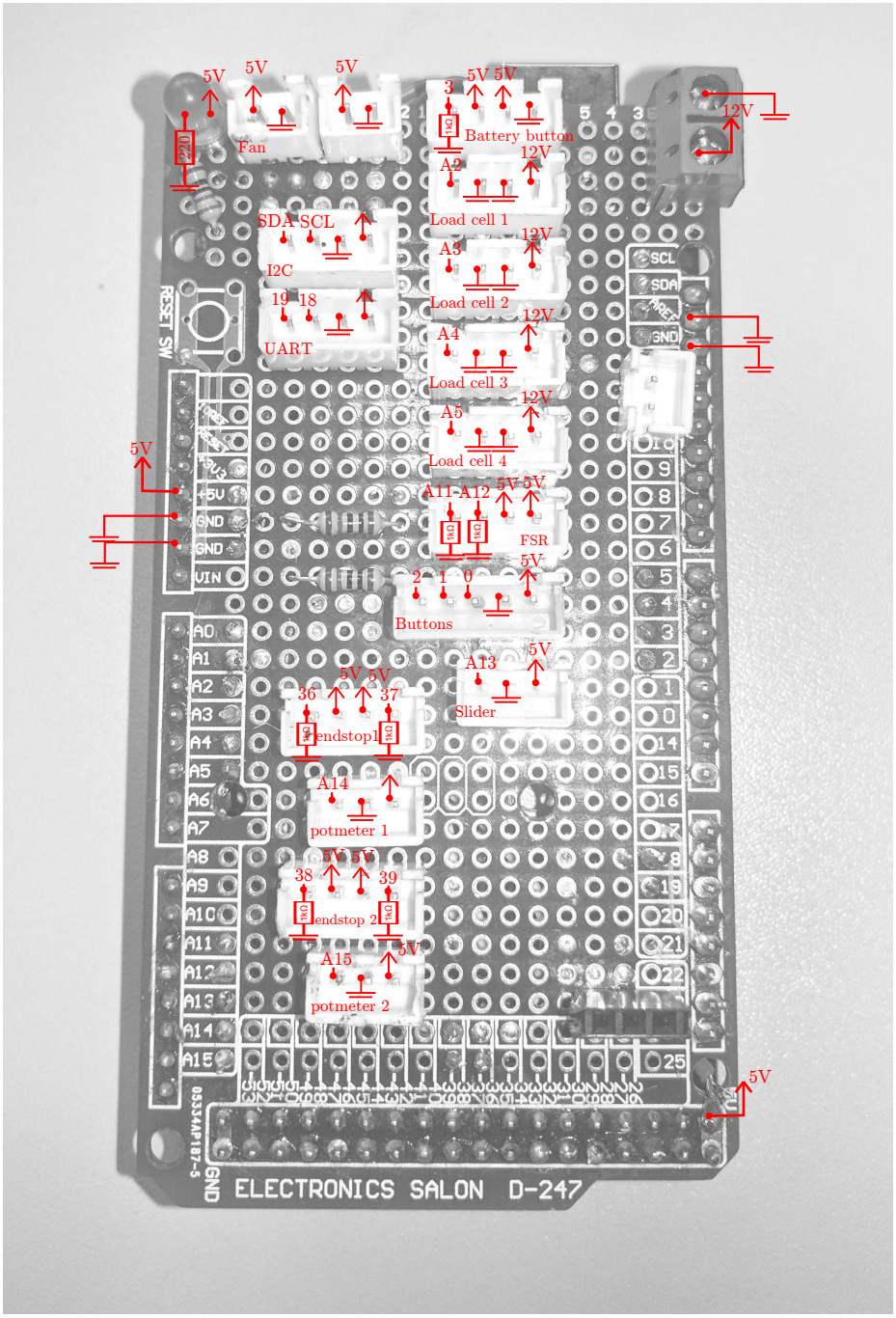

Figure 49: Custom made Arduino Mega shield pinout.

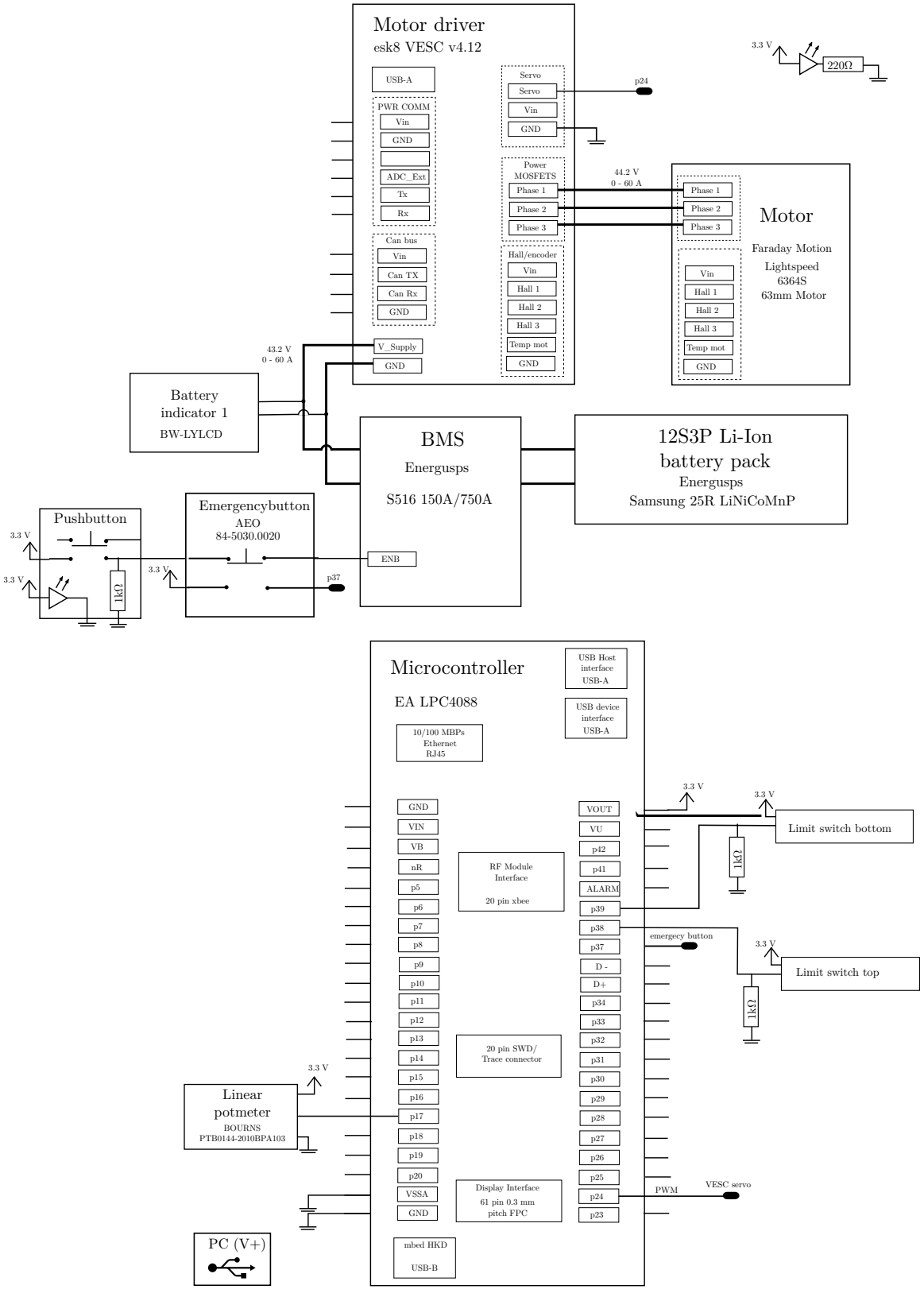

Figure 50: Electronic scheme AGB.